

Supplementary Materials for

Inborn errors of type I IFN immunity in patients with life-threatening COVID-19

Qian Zhang, Paul Bastard*, Zhiyong Liu*, Jérémie Le Pen*, Marcela Moncada-Velez*, Jie Chen*, Masato Ogishi*, Ira K. D. Sabli*, Stephanie Hodeib*, Cecilia Korol*, Jérémie Rosain*, Kaya Bilguvar*, Junqiang Ye*, Alexandre Bolze*, Benedetta Bigio*, Rui Yang*, Andrés Augusto Arias*, Qinhua Zhou*, Yu Zhang*, Fanny Onodi, Sarantis Korniotis, Léa Karpf, Quentin Philippot, Marwa Chbihi, Lucie Bonnet-Madin, Karim Dorgham, Nikaia Smith, William M. Schneider, Brandon S. Razooky, Hans-Heinrich Hoffmann, Eleftherios Michailidis, Leen Moens, Ji Eun Han, Lazaro Lorenzo, Lucy Bizien, Philip Meade, Anna-Lena Neehus, Aileen Camille Ugurbil, Aurélien Corneau, Gaspard Kerner, Peng Zhang, Franck Rapaport, Yoann Seeleuthner, Jeremy Manry, Cecile Masson, Yohann Schmitt, Agatha Schlüter, Tom Le Voyer, Taushif Khan, Juan Li, Jacques Fellay, Lucie Roussel, Mohammad Shahrooei, Mohammed F. Alosaimi, Davood Mansouri, Haya Al-Saud, Fahd Al-Mulla, Feras Almourfi, Saleh Zaid Al-Muhsen, Fahad Alsohime, Saeed Al Turki, Rana Hasanato, Diederik van de Beek, Andrea Biondi, Laura Rachele Bettini, Mariella D'Angio, Paolo Bonfanti, Luisa Imberti, Alessandra Sottini, Simone Paghera, Eugenia Quiros-Roldan, Camillo Rossi, Andrew J. Oler, Miranda F. Tompkins, Camille Alba, Isabelle Vandernoot, Jean-Christophe Goffard, Guillaume Smits, Isabelle Migeotte, Filomeen Haerynck, Pere Soler-Palacin, Andrea Martin-Nalda, Roger Colobran, Pierre-Emmanuel Morange, Sevgi Keles, Fatma Çölkesen, Tayfun Ozelik, Kadriye Kart Yasar, Sevtap Senoglu, Şemsi Nur Karabela, Carlos Rodríguez Gallego, Giuseppe Novelli, Sami Hraiech, Yacine Tandjaoui-Lambiotte, Xavier Duval, Cédric Laouénan, COVID-STORM Clinicians†, COVID Clinicians†, Imagine COVID Group†, French COVID Cohort Study Group†, CoV-Contact Cohort†, Amsterdam UMC Covid-19 Biobank†, COVID Human Genetic Effort†, NIAID-USUHS/TAGC COVID Immunity Group†, Andrew L. Snow, Clifton L. Dalgard, Joshua Milner, Donald C. Vinh, Trine H. Mogensen, Nico Marr, András N. Spaan, Bertrand Boisson, Stéphanie Boisson-Dupuis, Jacinta Bustamante, Anne Puel, Michael Ciancanelli, Isabelle Meyts, Tom Maniatis, Vassili Soumelis, Ali Amara, Michel Nussenzweig, Adolfo García-Sastre, Florian Krammer, Aurora Pujol, Darragh Duffy, Richard Lifton‡, Shen-Ying Zhang‡, Guy Gorochoff‡, Vivien Béziat‡, Emmanuelle Jouanguy‡, Vanessa Sancho-Shimizu‡, Charles M. Rice‡, Laurent Abel‡, Luigi D. Notarangelo§, Aurélie Cobat§, Helen C. Su§, Jean-Laurent Casanova§¶

*These authors contributed equally to this work.

†All collaborators and their affiliations appear at the end of this paper.

‡These authors contributed equally to this work.

§These authors contributed equally to this work.

¶Corresponding author. Email: casanova@rockefeller.edu

Published 24 September 2020 on *Science* First Release
DOI: 10.1126/science.abd4570

This PDF file includes:

Materials and Methods
Figs. S1 to S11
Tables S1 and S2
References

Other Supplementary Material for this manuscript includes the following:
(available at science.sciencemag.org/cgi/content/full/science.abd4570/DC1)

MDAR Reproducibility Checklist (PDF)

Materials and Methods

Patients

We included in this study 659 patients with life-threatening COVID-19 pneumonia defined as patients with pneumonia who developed critical disease, whether pulmonary with mechanical ventilation (CPAP, BIPAP, intubation, hi-flow oxygen), septic shock, or with any other organ damage requiring admission to the ICU. Patients who developed Kawasaki-like syndrome were excluded. The age of the patients ranged from 0.1-99 years, with a mean age of 51.8 years (SD 15.9 years), and 25.5% of the patients were female. As controls, we enrolled 534 individuals infected with SARS-CoV-2 (based on a positive PCR and/or serological test and/or the presence of typical symptoms such as anosmia/ageusia after exposure to a confirmed COVID-19 case) who remained asymptomatic or developed mild, self-healing, ambulatory disease.

All enrolled subjects provided written informed consent and were collected through protocols following local ethics recommendations. For patients enrolled in the French COVID cohort (clinicaltrials.gov NCT04262921), ethics approval was obtained from the CPP IDF VI (ID RCB: 2020-A00256-33). Ethics approval was obtained from the Ethics Committee of Erasme Hospital (P2020/203). For subjects enrolled in the COV-Contact study (clinicaltrials.gov NCT04259892), ethics approval was obtained from the CPP IDF VI (ID RCB: 2020-A00280-39). For patients enrolled in the Italian cohort, ethical approval was obtained from the University of Milano-Bicocca School of Medicine, San Gerardo Hospital, Monza – Ethics Committee of the National Institute of Infectious Diseases Lazzaro Spallanzani (84/2020) (Italy), and the Comitato Etico Provinciale (NP 4000 – Studio CORONAlab). STORM-Health care workers were enrolled in the STudio OsseRvazionale sullo screening dei laboratori ospedalieri per COVID-19 (STORM-HCW) study and approved by the local IRB on June 18th 2020. Anonymized samples were sequenced at the NIAID under non-human subject research conditions; no additional IRB consent was required at the NIH.

Next-generation sequencing

Genomic DNA was extracted from whole blood. For the 1193 patients and controls included, the whole exome ($N=687$) or whole genome ($N=506$) was sequenced at several sequencing centers, including the Genomics Core Facility of the Imagine Institute (Paris, France), the Yale Center for Genome Analysis (USA), the New-York Genome Center (NY, USA), and the American Genome Center (TAGC, USUHS, Bethesda, USA). For WES, libraries were generated with the Twist Bioscience kit (Twist Human Core Exome Kit), the xGen Exome Research Panel from Integrated DNA Technologies (IDT xGen), the Agilent SureSelect V7 kit or the SeqCap EZ MedExome kit from Roche. Massively parallel sequencing was performed on a NovaSeq6000 system (Illumina).

For WGS performed on Italian cohort patients (TAGC), genomic DNA samples were dispensed into the wells of a Covaris 96 microTUBE plate (1,000 ng per well) and sheared with the Covaris LE220 Focused-ultrasonicator, at settings targeting a peak size of 410 bp (t:78; Duty:18; PIP:450; 200 cycles). Sequencing libraries were generated from fragmented DNA with the Illumina TruSeq DNA PCR-Free HT Library Preparation Kit,

with minor modifications for automation (Hamilton STAR Liquid Handling System), with IDT for Illumina TruSeq DNA UD Index (96 indexes, 96 samples) adapters. Library size distribution and the absence of free adapters or adapter dimers were assessed by automated capillary gel electrophoresis (Advanced Analytical Fragment Analyzer). Library concentration was determined by qPCR with the KAPA qPCR Quantification Kit (Roche Light Cycler 480 Instrument II). Sequencing libraries were normalized and combined as 24-plex pools and quantified as above, before dilution to 2.9 nM and sequencing on an Illumina NovaSeq 6000 with a S4 Reagent Kit (300 cycles) and 151+8+8+151 cycle run parameters. Primary sequencing data were demultiplexed with the Illumina HAS2.2 pipeline and sample-level quality control was performed for base quality, coverage, duplicates and contamination (FREEMIX < 0.05 by VerifyBamID).

We used the Genome Analysis Software Kit (GATK) (version 3.4-46 or 4) best-practice pipeline to analyze our WES data (30). We aligned the reads obtained with the human reference genome (hg19), using the maximum exact matches algorithm in the Burrows–Wheeler Aligner (BWA) (31). PCR duplicates were removed with Picard tools (picard.sourceforge.net). The GATK base quality score recalibrator was applied to correct sequencing artifacts.

All the variants were manually curated using IGV and confirmed to affect the main functional protein isoform by checking the protein sequence before inclusion in further analyzes. The main functional protein isoforms are: TLR3 (NM_003265), UNC93B1 (NM_030930.4), TICAM1 (NM_182919), TRAF3 (NM_145725.2), TBK1 (NM_013254.4), IRF3 (NM_001571), IRF7 (NM_001572.5), IFNAR1 (NM_000629.3), IFNAR2 (NM_001289125.3), STAT1 (NM_007315.4), STAT2 (NM_005419.4), IRF9 (NM_006084.5). The analysis of IKBKG was customized to differentiate the duplicated region in IKBKG using a special pipeline previously described (32).

CNV detection

We searched the NGS data for deletions in the 13 genes of interest, using both the HMZDelFinder (33) and CANOES (34) algorithms.

Statistical analysis

We performed an enrichment analysis on our cohort of 659 patients with life-threatening COVID-19 pneumonia and 534 SARS-CoV2 infected controls, focusing on 12 autosomal IFN-related genes. We considered variants that were pLOF, with a MAF lower than 0.001 (gnomAD v2.1.1) after experimentally demonstrating that all the pLOF variants seen in the cases were actually LOF. We compared the proportion of individuals carrying at least one pLOF variant of the 12 autosomal genes in cases and controls by means of logistic regression with the likelihood ratio test. We accounted for the ethnic heterogeneity of the cohorts by including the first three principal components of the PCA in the logistic regression model. PC adjustment is a common and efficient strategy for accounting for different ancestries of patients and controls in the study of rare variants (35, 36, 37, 38). We checked that our adjusted burden test was well calibrated, by also performing an analysis of enrichment in rare (MAF < 0.001) synonymous variants of the 12 genes. PCA was performed with Plink v1.9 software on Whole-Exome and Whole-

Genome Sequencing data and 1000 Genomes (1kG) Project phase 3 public database as reference, using 27,480 exonic variants with a minor allele frequency > 0.01 and a call rate > 0.99. The odds ratio was also estimated by logistic regression and adjusted for ethnic heterogeneity.

TLR3 functional test

The TLR3-deficient P2.1 fibrosarcoma cell line was kindly provided by Douglas W. Leaman. Stably transfected P2.1 cells were established by transfection with pUNO-TLR3-HA (Invivogen, USA) in the presence of X-tremegene 9, with selection on blasticidin (10 µg/mL). The cells were stimulated with the TLR3 agonist poly(I:C) (Amersham) at a concentration of 25 µg/mL. After four hours of stimulation, the cells were harvested, and their cytokine mRNA production was analyzed by quantitative RT-qPCR, as previously described (6).

UNC93B1 expression test

UNC93B1-deficient SV40-Fib was transiently transfected wild-type and mutant pCMV6-UNC93B1 using X-tremeGENE 9 DNA transfection reagent following manufacturer's instruction. 48 hours after transfection, cells were harvested and whole cell lysates were prepared using RIPA buffer. Protein expression was assessed by western blotting.

TICAM1 functional test

TRIF^{-/-} SV40-Fib have been described elsewhere (9). The cells were transfected with pEF-BOS-TRIF plasmids (N-terminally tagged with HA), IFN-β-firefly luciferase and pRL-TK *Renilla* luciferase reporters, with Lipofectamine 3000 (Invitrogen). Reporter activity was measured 24 hours after transfection, with the Dual-Luciferase Reporter Assay System (Promega Corporation), according to the manufacturer's instructions. Firefly luciferase activity was normalized against *Renilla* luciferase activity and expressed as a fold-change relative to cells transfected with the wild-type construct.

HEK-Blue Null1-k cells (Invivogen) expressing the NF-κB SEAP reporter were transfected with pEF-BOS-TRIF plasmids, with Lipofectamine 2000. SEAP activity was assessed 24 hours after transfection, according to the manufacturer's instruction.

TRAF3 functional test

TRAF3-deficient HEK293T cells were kindly provided by Dr. Maria Romanelli (39). They were transiently transfected with pCMV6-TRAF3 wildtype and mutants plasmids, with Lipofectamine LTX, according to the manufacturer's instructions, and were cotransfected with the NF-κB-firefly luciferase reporter plasmid and the pRL-TK-*Renilla* luciferase plasmid. Luciferase activity was measured 24 hours after transfection, with the Dual-Luciferase Reporter Assay System. Firefly luciferase activity was first normalized against *Renilla* luciferase activity, and then against empty vector. TRAF3 expression was measured by western blotting (anti-TRAF3 antibody, Abcam, Cambridge, MA, USA).

TBK1 functional test

HEK293T cells were transfected with pCDNA3-TBK1 plasmids, with Lipofectamine 2000, together with IFN- β -firefly and pRL-TK *Renilla* luciferase reporter constructs. Reporter activity was measured 24 hours after transfection, with the Dual-Luciferase Reporter Assay System. Firefly luciferase activity was normalized against *Renilla* luciferase activity and expressed as a fold-change relative to cells transfected with the empty vector.

IRF3 functional test

IRF3-deficient HEK293T cells were cotransfected with a mixture of the IFN- β -firefly luciferase reporter plasmid, the pRL-TK-*Renilla* luciferase plasmid, and the pCDNA3-IRF3 plasmid. Cells were incubated for 24 hours after transfection, and were then either left untreated or infected with Sendai virus (20 HAU/well) for another 24 hours. Reporter activity was measured with the Dual-Luciferase Reporter Assay System. Firefly luciferase activity was normalized against *Renilla* luciferase activity.

IRF3 c.438C>G/p.N146K exon trapping

DNA segments encompassing the *IRF3* exon 4 to 6 region (from chr19:50166562 to chr19:50164806 – GRCh37 reference) were amplified from genomic DNA and inserted into a pSPL3 vector, between the *EcoRI* and *BamHI* sites. Wild-type and mutant (*IRF3* c.438C>G, a missense variant located in exon 5 and predicted to activate a cryptic splicing donor site), plasmids were used to transfect COS-7 cells. After 24 h, total RNA was extracted and reverse-transcribed. The *IRF3* splicing products were amplified with flanking HIV-TAT sequences from the pSPL3 vector and ligated into the pCR4-TOPO vector (Invitrogen). Stellar cells (Takara) were transformed with the resulting plasmids. Colony PCR and sequencing with primers located in the flanking HIV-TAT sequences of pSPL3 were performed to determine the splicing products produced by the WT and mutated alleles.

IRF7 functional test

HEK293T cells were cotransfected with a mixture of the IFN- β -firefly luciferase reporter plasmid, the pRL-TK-*Renilla* luciferase plasmid, and the pCDNA3-IRF7 plasmid. Cells were incubated for 24 hours and were then either left untreated or infected with Sendai virus (20 HAU/well) for another 24 hours. Reporter activity was measured with the Dual-Luciferase Reporter Assay System. Firefly luciferase activity was normalized against *Renilla* luciferase activity. IRF7 expression levels were measured by western blotting (anti-IRF7 antibody: Cell Signaling, Danvers, MA; anti-FLAG antibody: Sigma).

IFNAR1 and IFNAR2 functional test

IFNAR1- or IFNAR2-deficient SV40-Fib were transfected with pCMV6-IFNAR1 or IFNAR2 plasmids, with Lipofectamine. Cells were incubated for 36 hours after transfection, and were then stimulated with IFN- α 2 (10,000 IU/mL) or - γ (10,000 IU/mL) for 15 minutes before staining. Intracellular staining of phosphorylated STAT1 was performed with an isotype control, according to the manufacturer's instructions. Results were analyzed with FlowJo.

STAT1 functional test

STAT1-deficient U3A cells were transfected with pCDNA3-STAT1, ISRE-firefly luciferase, and pRL-TK-*Renilla* luciferase reporter constructs, with Lipofectamine 3000 (Invitrogen). The cells were incubated for 24 hours after transfection, and were then stimulated with IFN- α for an additional 16 hours. Reporter activity was measured with the Dual-Luciferase Reporter Assay System (Promega Corporation), according to the manufacturer's instructions. Firefly luciferase activity was normalized against *Renilla* luciferase activity and expressed as a fold-change relative to cells transfected with the empty vector.

STAT2 functional test

STAT2 production and phosphorylation: HEK293T cells were transiently transfected with pCMV6-STAT2-mCherry plasmids, with Lipofectamine 2000. The cells were incubated for 24 hours after transfection, and were then stimulated with 10⁴ IU/mL IFN- α 2 (Thermo Fisher Scientific) for 30 minutes. Cell lysates were obtained by extraction in RIPA buffer. Total STAT2 (sc-514193, epitope 7-26 AA of N-terminus, Santa Cruz Biotechnology) and p-STAT2 (Y689 AF2890; R&D Systems) levels were determined by western blotting. HEK293T cells were transiently transfected with pCDNA3-STAT2, pCMV6-IRF9, ISRE-firefly luciferase, and pRL-TK-*Renilla* luciferase reporter plasmids. Reporter activity was measured with the Dual-Luciferase Reporter Assay System (Promega Corporation), according to the manufacturer's instructions.

IRF9 functional test

IRF9-deficient SV40-Fib was transiently transfected wild-type and mutant pCMV6-IRF9 using X-tremeGENE 9 DNA transfection reagent following manufacturer's instruction. 48 hours after transfection, cells were either left untreated or stimulated with 10,000 IU/mL IFN- α 2 for 8 hours before total RNA was extracted (Qiagen). mRNA levels of *IRF9*, *IFIT1*, and *IFI27* were measured with RT-qPCR (Taqman gene expression assay, ThermoFisher) according to manufacturer's instructions. IRF9 expression level was measured by western blotting (anti-IRF9 antibody: Santa Cruz Biotechnology).

PHA-T cells

PBMCs purified from whole blood were activated by incubation with phytohemagglutinin (PHA) (5 μ g/mL) and kept cycling for at least five days before experiments.

pDC purification

Peripheral blood mononuclear cells (PBMCs) were isolated by Ficoll density gradient centrifugation (Ficoll-Paque; GE Healthcare). Plasmacytoid DCs (pDCs) were sorted magnetically with the Human Plasmacytoid DC Enrichment Kit (Stem Cell), according to the manufacturer's instructions.

For the assessment of pDC enrichment, cells were stained with Zombie Violet fixable viability stain (Biolegend), FITC anti-CD16 (BD, clone NKP15), FITC anti-CD14 (Miltenyi Biotec, clone TŮK4), FITC anti-CD19 (Miltenyi Biotec, clone LT19), FITC anti-CD20 (BD, clone 2H7), FITC anti-CD56 (Biolegend, clone HCD56), FITC anti-CD3 (BD, clone HIT3a), BV650 anti-CD4 (Biolegend, clone OKT4), APC-Vio770 anti-CD2

(Miltenyi Biotec, clone LT2), APC anti-CD5 (BD, clone UCHT2), and BV785 anti-CD123 (Biolegend, clone 6H6) antibodies. PDCs were gated as Live, Lin⁻ (CD16, CD14, CD19, CD20, CD56 and CD3), CD2⁻ CD5⁻, and CD4⁺ CD123⁺ cells. Acquisitions were performed on an LSRFortessa machine (BD Biosciences). Data were analyzed with FlowJo software (TreeStar).

pDC activation by SARS-CoV-2 and cytokine production

pDCs from an IRF7^{-/-} patient and a healthy donor matched for age and sex were cultured at a density of 3 x 10⁵ and 5 x 10⁵ cells/mL, respectively, for 12 h, in the presence of medium alone (RPMI 1640 Medium with GlutaMAX, 10% FBS, 1% MEM NEAA, 1% sodium pyruvate, and 1% penicillin/streptomycin), influenza virus (Charles River, A/PR/8/34, 2 µg/mL), or the SARS-CoV-2 primary strain 220_95 (GISAID accession ID: EPI_ISL_469284) at a multiplicity of infection (MOI) of 2. This SARS-CoV-2 virus was isolated from nasopharyngeal swabs and amplified in Vero cells. After 12 hours of culture, pDC supernatant was collected for cytokine quantification. Supernatants were incubated for 2 hours at room temperature with 0.4% (v/v) Triton X-100 before quantification, to inactivate the infectious particles of SARS-CoV-2. IFN-α2 levels were measured in BD cytometric bead arrays (CBAs), in accordance with the manufacturer's protocol, with a 20 pg/mL detection limit. Acquisitions were performed on an LSRFortessa machine (BD Biosciences), and cytokine concentration was determined with FCAP Array Software (BD Biosciences). IFN-λ1 secretion was measured in an enzyme-linked immunosorbent assay (ELISA) (R&D Systems, DuoSet DY7246), in accordance with the manufacturer's instructions. The optical density (OD) of the supernatant was defined as its absolute OD value, minus the OD for the blank wells. The detection limit was 85 pg/mL and all samples were run in duplicate. Optical density was measured on a CLARIOstar Plus microplate reader (BMG Labtech).

SARS-CoV-2 infection in patient SV40-Fib

Patient SV40-Fib cells were cultured in DMEM with 10% fetal calf serum. To make patients-derived fibroblasts permissive to SARS-CoV-2 infection, we delivered human ACE2 and TMPRSS2 cDNA to cells by lentivirus transduction using a modified SCRPSY vector (GenBank: KT368137.1). The pSCRPSY_TMPRSS2-2A-NeoR_ACE2 construct was made by cloning the ACE2 open reading into the multiple cloning region and by replacing the PAC (puromycin acetyl transferase) 2A (stop-start/skip from FMDV) TagRFP (red fluorescent protein) cassette with a TMPRSS2-2A-NeoR (neomycin phosphotransferase II; NPT II) cassette. The pSCRPSY_TMPRSS2-2A-NeoR_ACE2 plasmid sequence is available upon request. To produce SCRPSY_TMPRSS2-2A-NeoR_ACE2 Lentivirus, Lenti-XTM cells 293T cells (Takara, cat. #632180) were seeded in 25 ml Dulbecco's Modified Eagle Medium (DMEM, Fisher Scientific, cat. #11995065) supplemented with 0.1 mM nonessential amino acids (NEAA, Fisher Scientific, cat. #11140076) and 3% fetal bovine serum (FBS, HyClone Laboratories, Lot. #AUJ35777) at 6.25 x 10⁶ per dish in two poly-L-lysine coated p150 dishes. The following day media was removed and replaced with 20 ml fresh media and each plate was transfected with 31.3 µg pSCRPSY_TMPRSS2-2A-NeoR_ACE2 plasmid, 15.6 µg VSV-G plasmid, and 23.4 µg HIV Gag-Pol using LipofectamineTM 2000 (Fisher Scientific, cat. #11668019) at 2.2 µl per µg DNA ratio supplemented with PLUSTM

Reagent (Fisher Scientific, cat. #11514015) at 4.4 µl per µg DNA diluted in 6 ml Opti-MEM Reduced Serum Medium (Fisher Scientific, cat. #51985034). Six hours post transfection media was removed, and lentivirus was collected overnight in 30 ml per plate fresh media. Twenty-four hours later lentivirus-containing media was collected, clarified by centrifugation at 500 x g for 5 min, filtered through a 0.22 µm filter (Corning, cat. #431153) and concentrated 50 times in Opti-MEM using Lenti-X™ concentrator (Takara, cat. #631232) following the manufacturer's instructions. SCRPSY_TMPRSS2-2A-NeoR_ACE2 Lentivirus was used on SV40-immortalized fibroblasts. 3.5x10⁵ cells were resuspended in transduction media (DMEM; 10% FBS; 8 µg/ml polybrene) and placed in 12-well plates. 10 µl of lentivirus (or 10 µl of Opti-MEM for mock control) was added to the cells still in suspension and the mixture was centrifuged for one hour at 1000 g at 37 °C. The cells were then cultured for one week with daily media change prior to SARS-CoV-2 infection.

SARS-CoV-2, strain USA-WA1/2020, was obtained from BEI Resources. Passage 1 virus, used in these studies, was produced by infecting Huh7.5 cells at MOI 0.05 and placing at 33 °C. Virus was harvested once >70% CPE was observed, about 5 days post infection. Viral titers were measured on Huh-7.5 cells by standard plaque assay where 400 µl of serial tenfold virus dilutions in Opti-MEM were used to infect 400,000 cells seeded the previous day in a 6-well plate format. After 60 min adsorption, the virus inoculum was removed, and cells were overlaid with DMEM containing 10% FCS with 1.2% microcrystalline cellulose (Avicel). Cells were incubated for 5 days at 33 °C, followed by fixation with 3.5% formaldehyde and crystal violet staining for plaque enumeration. All SARS-CoV-2 experiments were performed in a biosafety level 3 (BSL3) laboratory.

ACE2/TMPRSS2-transduced cells were seeded at 10,000 cells per well in optical-grade 96-well plates (Corning, cat. #3904) and incubated for three days at 37°C. Cells were pre-treated with or without 500 U/ml IFN-β (PBL Assay Science, cat. #11415-1) four hours prior to infection. Media was then discarded and cells infected with SARS-CoV-2 diluted in Opti-MEM (MOI=0.5 determined on Huh7.5 cells) for one hour at 37 °C in 50 µl of inoculum. After virus inoculation, cells were washed twice with culture media and incubated at 37 °C with 200 µl of fresh culture media. After 24 hours of infection, cells were fixed with 4% formaldehyde for one hour. The plates were thoroughly washed with 70% ethanol and taken out of the BSL3 for staining.

After fixation, cells were washed twice with PBS, permeabilized with a 0.1% triton in PBS solution for 15 minutes, blocked with 4% FBS in PBS solution for one hour, and incubated with SARS-CoV-2 and ACE2 primary antibodies (0.5 µg/ml and 1 µg/ml, respectively) for one hour at room temperature. Primary antibodies: SARS-CoV-2, human monoclonal anti-Spike-SARS-CoV-2 C121 (40); ACE2, mouse monoclonal Alexa Fluor 488-conjugated Antibody (R&D systems, cat. # FAB9332G-100UG). Cells were washed twice with PBS and incubated with 1 µg/ml secondary antibodies and Hoechst 33342 (Invitrogen, cat. #H3570) for thirty minutes at room temperature: Goat anti-Human IgG (H+L) Cross-Adsorbed Secondary Antibody, Alexa Fluor 647 (Invitrogen, cat. # A-21445), Goat anti-Mouse IgG (H+L) Cross-Adsorbed Secondary

Antibody, Alexa Fluor 488 (Invitrogen, cat. # A-11001). Cells were washed three times with PBS and imaged. Images were acquired with an ImageXpress Micro XLS microscope (Molecular Devices) using the 4X objective. The MetaXpress software (Molecular Devices) produced single cell mean fluorescence intensity (MFI) values.

Data analysis on single cell MFI values was done in the R environment (v4.0.2). ACE2/TMPRSS2-transduced cells were classified ACE2 positive when the ACE2 log MFI was superior to the log mean MFI of mock-transduced cells plus 2.5 standard deviations. We excluded all wells with less than 150 ACE2-positive cells before SARS-CoV-2 scoring. ACE2-expressing cells were classified SARS-CoV-2 positive when the fluorescence intensity value was superior to the mean fluorescence intensity of mock-infected cells plus 4 standard deviations. The median SARS-CoV-2 MFI and percentage SARS-CoV-2 positive cells were calculated for each well (independent infection).

Single-molecule array (Simoa) IFN- α digital ELISA

Serum IFN- α concentrations were determined with Simoa technology, with reagents and procedures obtained from Quanterix Corporation (Quanterix SimoaTM IFN α Reagent Kit, Lexington, MA, USA). According to the manufacturer's instructions, the working dilutions were 1:2 for all sera, in working volumes of 170 μ L. In the first step of the assay, capture beads coated with an anti-cytokine Ab were combined with the serum. After washing, the biotinylated detector Ab was added to the reaction to bind the captured cytokine. Following a second wash, streptavidin- β -galactosidase (SBG) was added to bind the detector Ab, resulting in enzyme labeling of the captured cytokine. After washing, the beads were resuspended in a resorufin β -D-galactopyranoside (RGP) substrate solution and immediately transferred to a Simoa disc array (Quanterix SimoaTM Disc Kit) for individual capture in the microwells. The β -galactosidase on the captured cytokine hydrolyzed the RGP substrate, yielding a fluorescent signal, for IFN α determination. At low cytokine concentrations, the percentage of bead-containing wells in the array displaying a positive signal is proportional to the amount of cytokine present in the sample (digital measurement). At higher concentrations, when most of the bead-containing wells have at least one labeled cytokine molecule, the total fluorescence signal is proportional to the amount of cytokine present in the sample (analog measurement). Cytokine concentrations in serum samples were interpolated from standard curves.

Mass cytometry

Mass cytometry was performed with the Maxpar Direct Immune Profiling Assay (Fluidigm) according to the supplier's instructions, with freezing at -80°C after the overnight dead-cell staining step, and acquisition on a Helios machine (Fluidigm). After manually excluding dead cells, doublets, and granulocytes, the remaining cells from the two IRF7 patients and 14 controls studied across five batches of experiments were identified through batch-corrected unsupervised clustering (41). We randomly selected 50,000 cells per individual to generate uniform manifold approximation and projection (UMAP) plots.

Influenza virus protein

Influenza virus protein microarrays (IVPM) were produced by spotting recombinant influenza virus hemagglutinins (HAs) onto epoxysilane-coated glass slides (Schott, Mainz, Germany), as previously described (42). Each microarray slide contained 24 identical arrays, consisting of 13 HAs diluted in 0.1% milk in PBS, printed in triplicate, at a volume of 30 nL per spot, at a concentration of 100 µg/mL. Three different array designs were included in this study. IVPs were vacuum-packed and stored at -80°C until use. Before use, IVP slides were warmed to room temperature. They were then incubated in a chamber maintained at 95-98% relative humidity for 2 hours, to bind proteins to the slide and inactivate epoxysilane residues not in contact with recombinant HAs. The IVP slides were then inserted into 96-well microarray gaskets (Arrayit, Sunnyvale, CA, USA), dividing each slide into 24 separate arrays. These arrays were blocked by incubation with 220 µL 3% milk in PBS supplemented with 0.1% Tween 20 (PBS-T) for 2 hours. The blocking solution was then removed from the arrays, and serum samples diluted 1:100 in 1% milk in PBS-T were incubated with the arrays at a volume of 100 µL and diluted 1:10 across three arrays. IVP arrays were washed three times with 220 µL PBS-T, and then 50 µL of Cy5-labeled anti-human IgG secondary antibody diluted 1:3000 in 1% milk in PBS-T was added to each array and the array was incubated for one hour. The secondary antibody solution was removed, each array was washed three times with PBS-T and the slides were removed from their gaskets for rinsing with PBS-T and deionized water. They were then dried with an air compressor. Arrays were imaged with a Videa microarray scanner (Indevr, Boulder, CO, USA), using an exposure time of 1000 ms. The area under the curve was calculated from the median spot fluorescence, taking the total peak area with a minimum threshold of 0.04.

Supplementary figures and tables

Fig. S1. Impact of TLR3, UNC93B1, and TICAM1 variants on expression and function. (A) TLR3 protein levels in P2.1 cells stably transfected with wild-type or mutant forms of *TLR3*, measured by western blotting. (B) UNC93B1-deficient SV40-Fib were transiently transfected with wild-type or mutant *UNC93B1*. Protein levels were measured by western blotting, 48 hours post transfection. (C) HEK-Blue-Null1-k (NF-kappaB/SEAP) cells were transiently transfected with wild-type or mutant *TICAM1*. SEAP levels were measured 24 hours after transfection. (D) TICAM1/TRIF proteins levels in TICAM1-deficient SV40-Fib transiently transfected with wild-type or mutant *TICAM1*, as measured by western blotting. NT: non-transfected; EV: empty vector, WT: wild-type. Variants in red were identified in COVID-19 patients. Variants in blue are known deleterious variants, which served as negative controls. Horizontal dash lines indicate cutout. Mean and standard deviation (SD) were shown in column and horizontal bars when appropriate. Three technical repeats were performed.

Fig. S2. Impact of TRAF3 and TBK1 variants on expression and function. (A) Levels of TRAF3 protein in TRAF3-deficient HEK293T cells transiently transfected with DDK-tagged wild-type or mutant *TRAF3*, as determined by western blotting. Separate blots were probed with anti-DDK and anti-TRAF3 antibodies. (B) TRAF3-deficient

HEK293T cells were transiently transfected with wildtype or mutant *TRAF3*, together with an NF- κ B luciferase reporter and a constitutively expressed reporter. Normalized luciferase activity was measured 24 hours after transfection. (C) *TBK1* was overexpressed in HEK293T cells. Total and phosphorylated TBK1, and total and phosphorylated IRF3 levels were measured by western blotting. NT: non-transfected; EV: empty vector, WT: wild-type. Variants in red were identified in COVID-19 patients. Variants in blue are known deleterious variants, which served as negative controls. Horizontal dash lines indicate cutout. Mean and standard deviation (SD) were shown in column and horizontal bars when appropriate. Three technical repeats were performed.

Fig. S3. Impact of IRF3 variants on expression and function. (A) IRF3-deficient HEK293T cells were transiently transfected with various amounts of plasmids encoding FLAG-tagged wildtype and mutant IRF3, and protein levels were measured by western blotting. (B) Exon trapping of the IRF3 variant (c.438C>G). E.V: exon 5.

Fig. S4. Impact of IRF7 variants on expression. HEK293T cells were transiently transfected with FLAG-tagged wild-type and mutant *IRF7*, and protein levels were measured by western blotting. EV: empty vector, WT: wild-type. Variants in red were identified in COVID-19 patients. Variants in blue are known deleterious variants, which served as negative controls. Vertical dash lines indicate gel cutout.

Fig. S5. Impact of IFNAR1 and IFNAR2 variants on expression. HEK293T cells were transiently transfected with wild-type and mutant *IFNAR1* (A) or *IFNAR2* (B) for 36 hours. Cell surface expression of IFNAR1 and IFNAR2 were measured by FACS staining and accessed by mean fluorescence intensity (MFI). Variants in red were identified in COVID-19 patients. Variants in blue are known deleterious variants, which served as negative controls.

Fig. S6. Impact of STAT1 variants on expression and function. (A) STAT1 protein levels in STAT1-deficient U3A cells transiently transfected with wild-type or mutant *STAT1* and stimulated with IFN- α 2. (B) U3A cells were transiently transfected with wildtype or mutant *STAT1*, together with an ISRE-luciferase reporter and a constitutively expressed reporter. Cells were either left untreated or were stimulated with IFN- α 2 for 16 hours, and normalized luciferase activity was then measured.

Fig. S7. Impact of STAT2 variants on expression and function. (A) STAT2 protein levels in 293T cells transiently transfected with wild-type or mutant *STAT2* and either left untreated or stimulated with IFN- α 2. Total STAT2 and p-STAT2 protein levels were measured by western blotting. (B) 293T cells were transiently transfected with wild-type or mutant *STAT1*, wild-type or mutant (deletion of exon 7) *IRF9*, ISRE luciferase reporter, and a constitutively expressed reporter. 24 hours after transfection, normalized luciferase activity was measured. WT: wild-type. Variants in blue are known deleterious variants, which served as negative controls.

Fig. S8. Impact of IRF9 variants on expression and function. (A) IRF9 protein levels in IRF9-deficient SV40-Fib cells transiently transfected with wild-type or mutant *IRF9*,

as measured by western blotting. **(B)** IRF9-deficient SV40-Fib cells transiently transfected with wild-type or mutant *IRF9*. 48 hours after transfection, cells were then either left untreated or stimulated with IFN- α 2 for 8 hours. Normalized *IRF9*, *IFIT1*, and *IFI27* transcript levels were determined by RT-qPCR. NT: non-transfected; EV: empty vector, WT: wild-type. Variants in red were identified in COVID-19 patients. Variants in blue are known deleterious variants, which served as negative controls.

Fig. S9. Peripheral pDC in patients with IRF7 deficiency. **(A)** Purity of pDCs isolated from a healthy donor (C) and a patient with AR IRF7 deficiency, as evaluated by FACS, after staining. **(B)** Mass cytometry on whole blood from a patient with AR IRF7 deficiency, a patient with AD IRF7 deficiency, and healthy donors (C1-3). Uniform Manifold Approximation and Projection (UMAP) were plotted in 2-dimension figure. Experiments #1 and #2 were performed on different days.

Fig. S10. IAV exposure in a patient with AR IRF7 deficiency. **(A)** Influenza virus protein microarrays (IVPM) in the plasma of the patient and controls. Frozen Belgian controls: C1-10 are sex and age matched healthy donors living in the same region of Belgium as the patient. **(B)** IAV strains corresponding to the viral protein identified in (A).

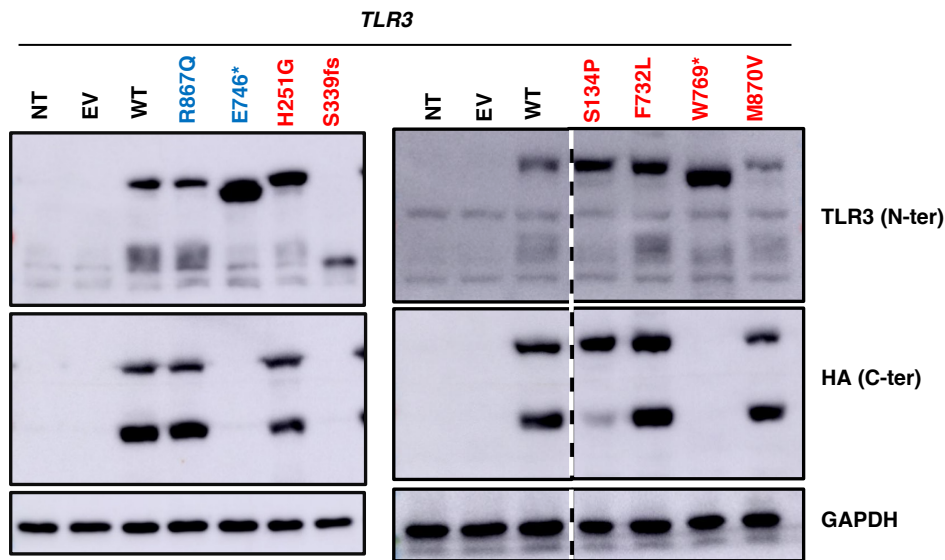
Fig. S11. Virscan analysis of a patient with an AR IRF7 deficiency. Plasma samples from the patient, family members, and controls (C1-20) were subjected to Virscan analysis. Common species scores are shown. Plasma from heterozygous carriers (father, mother, and brother) and wild-type sister were tested in the same experiment. IgG depleted plasma, IVIG, and travel controls served as technical controls.

Table S1. Variants of the 12 autosomal loci identified in patients with life-threatening COVID-19. Variants with a MAF<0.001 are listed. pLOF: predicted loss-of-function; LOF: loss-of-function; HYPO: severely hypomorphic; LOE: loss-of-expression.

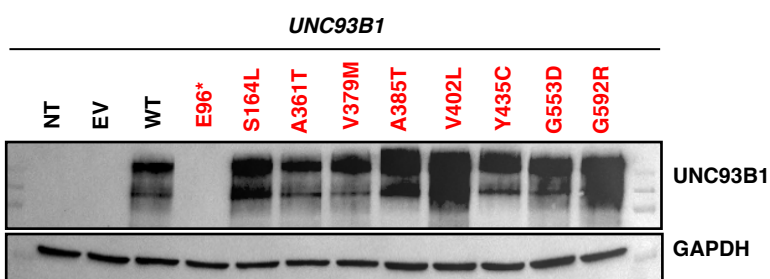
Table S2. Variants identified in the 417 known IEI-causing genes in patients with defects of the type I IFN pathway.

Fig. S1. Impact of TLR3, UNC93B1, and TICAM1 variants on expression and function.

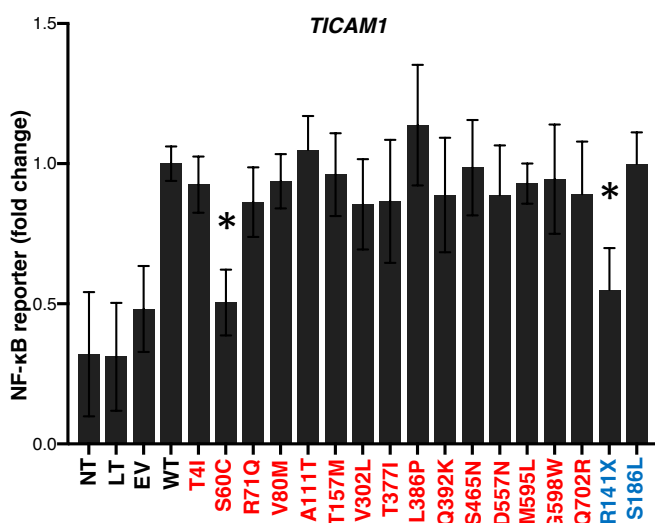
A



B



C



D

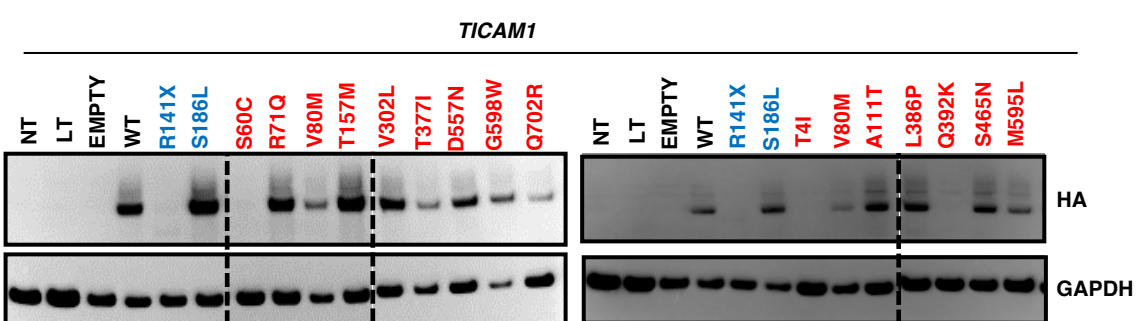
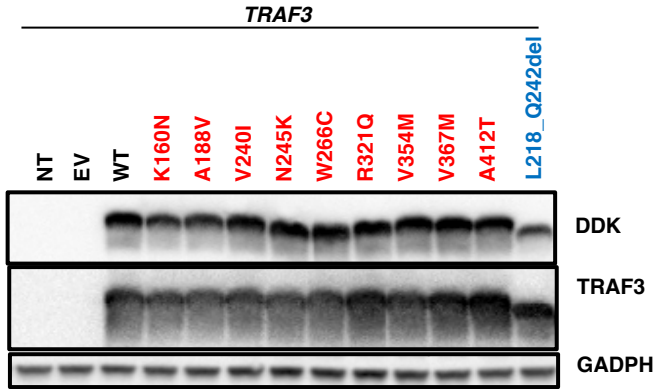
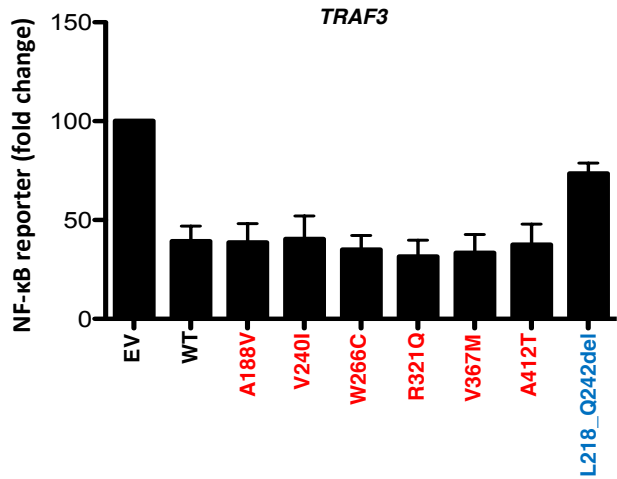


Fig. S2. Impact of TRAF3 and TBK1 variants on expression and function.

A



B



C

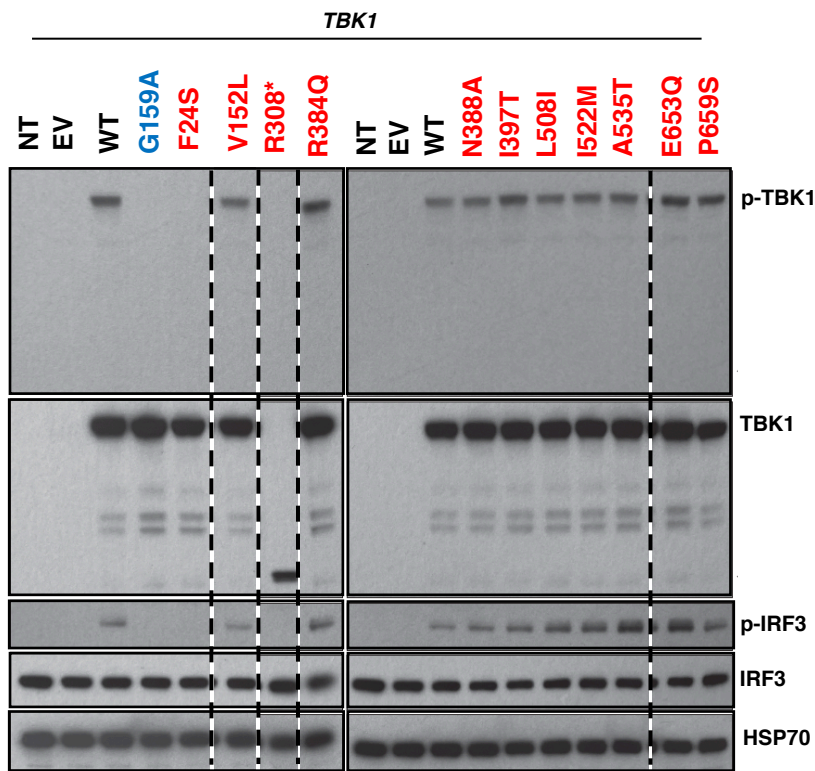
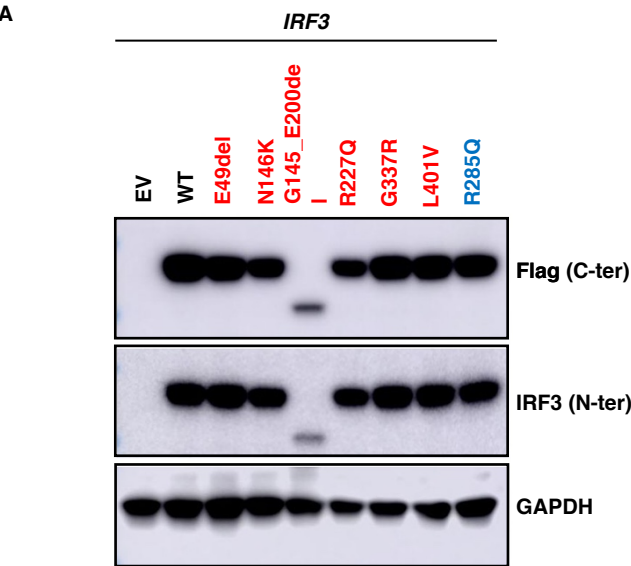


Fig. S3. Impact of IRF3 variants on expression and function.



B

		c.438C>G products count	
		Mutant	WT
N146K	HIV tat E. V HIV tat	19	46
	HIV tat HIV tat	4	8
G145_E200del	HIV tat HIV tat	35	0
	HIV tat HIV tat	1	0
	HIV tat HIV tat	1	3

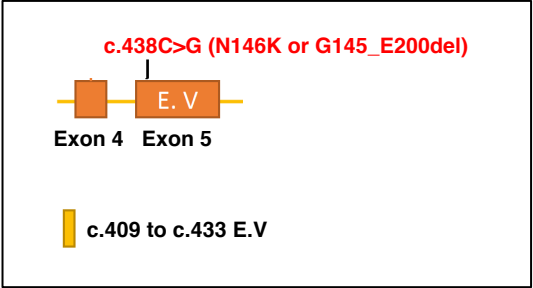


Fig. S4. Impact of IRF7 variants on expression.

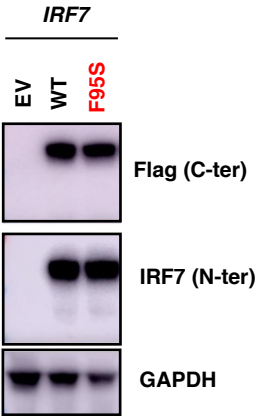
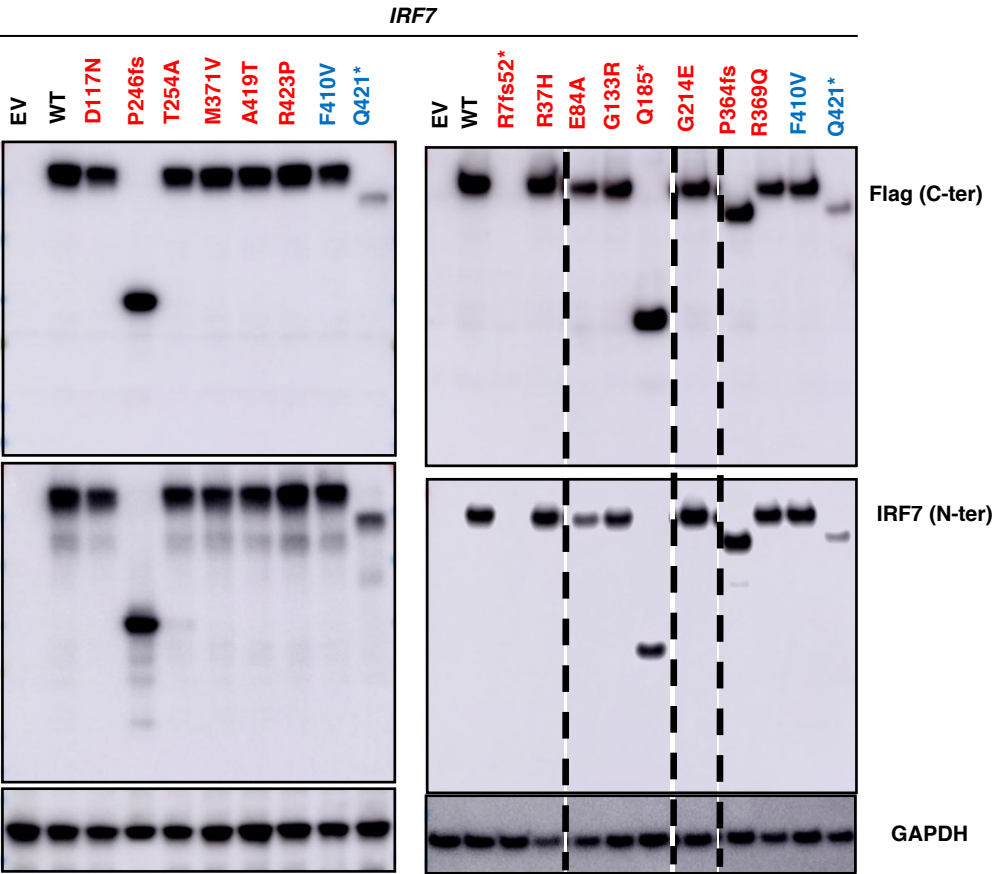
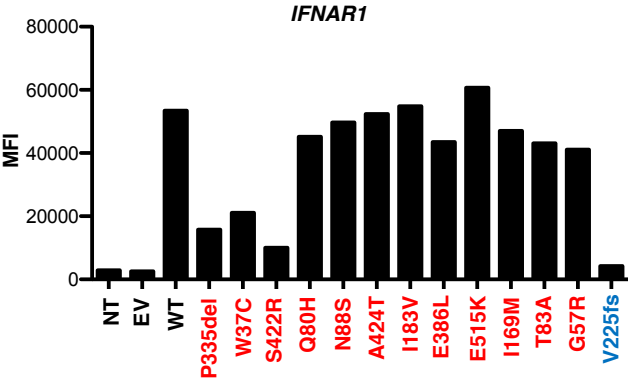


Fig. S5. Impact of IFNAR1 and IFNAR2 variants on expression.

A



B

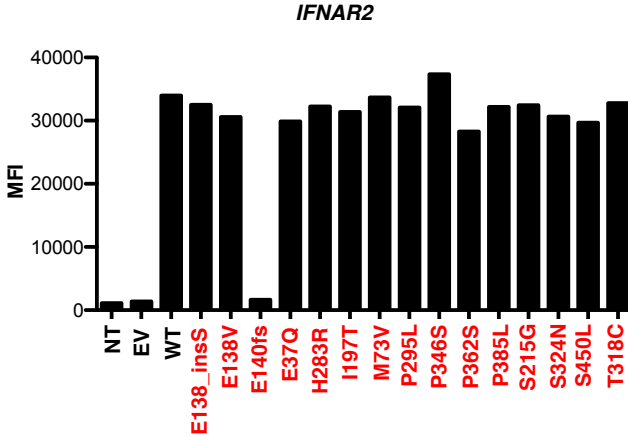


Fig. S6. Impact of STAT1 variants on expression and function.

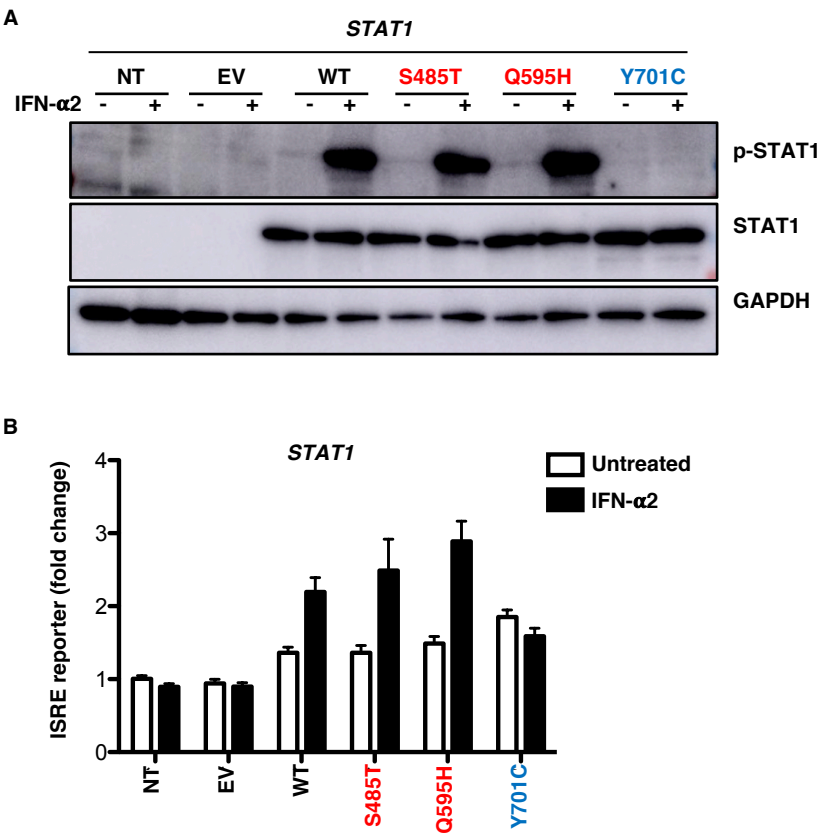
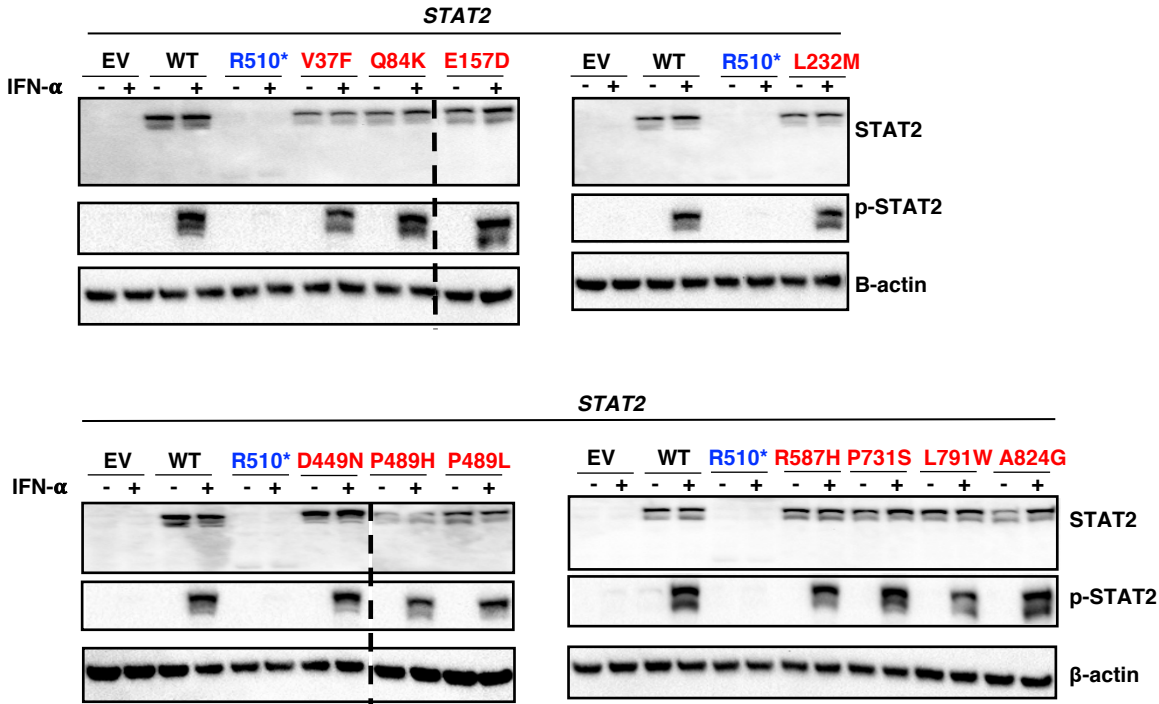


Fig. S7. Impact of STAT2 variants on expression and function.

A



B

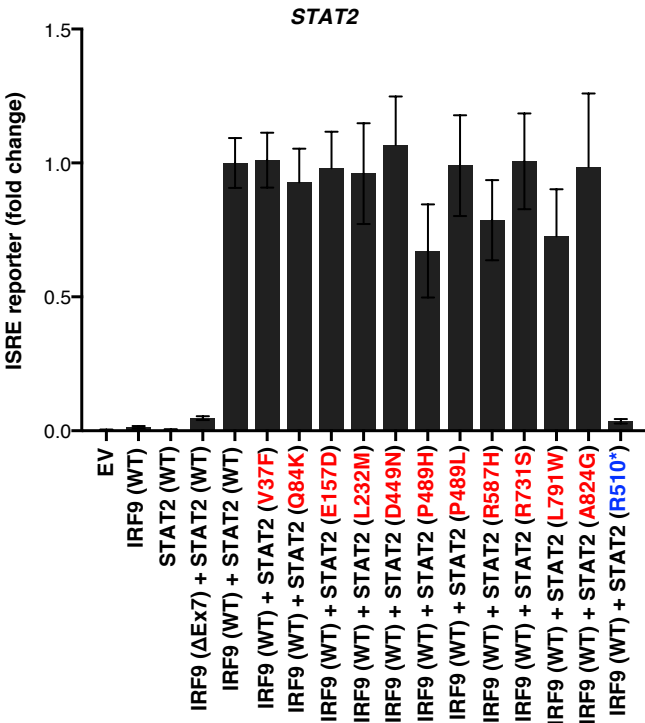


Fig. S8. Impact of IRF9 variants on expression and function.

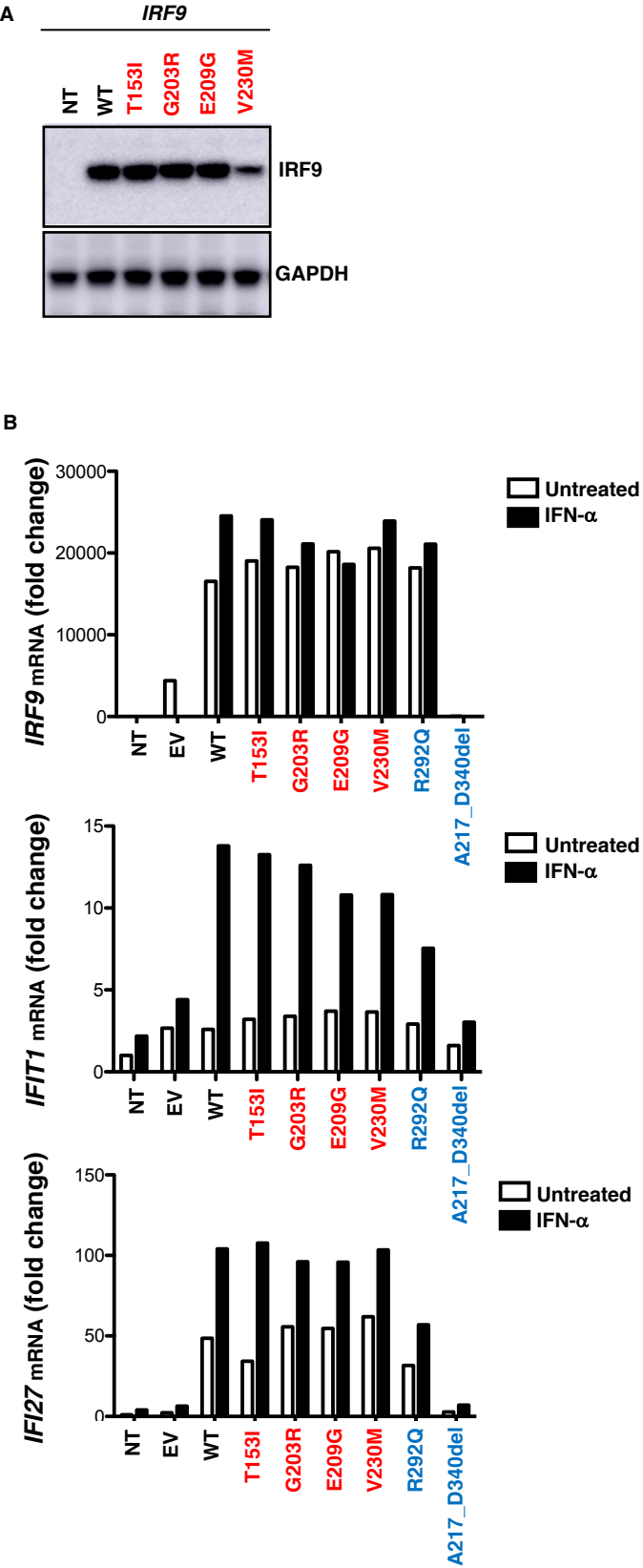
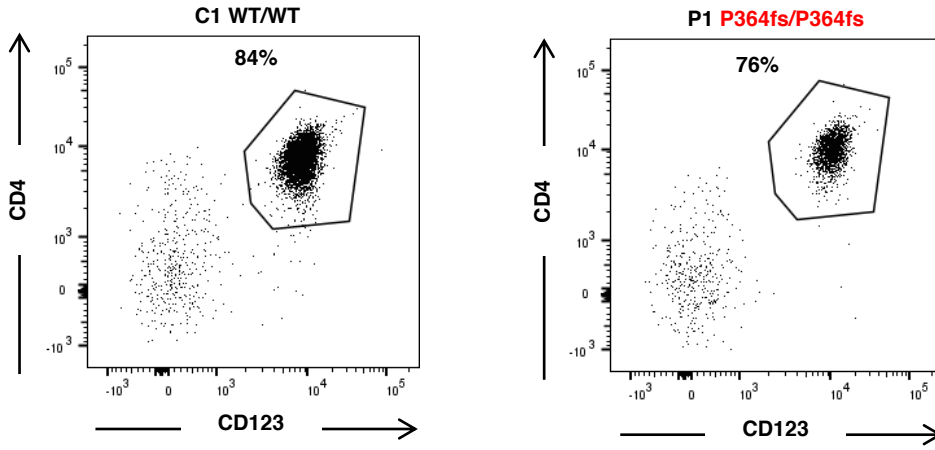


Fig. S9. Peripheral pDC in patients with IRF7 deficiency.

A



B

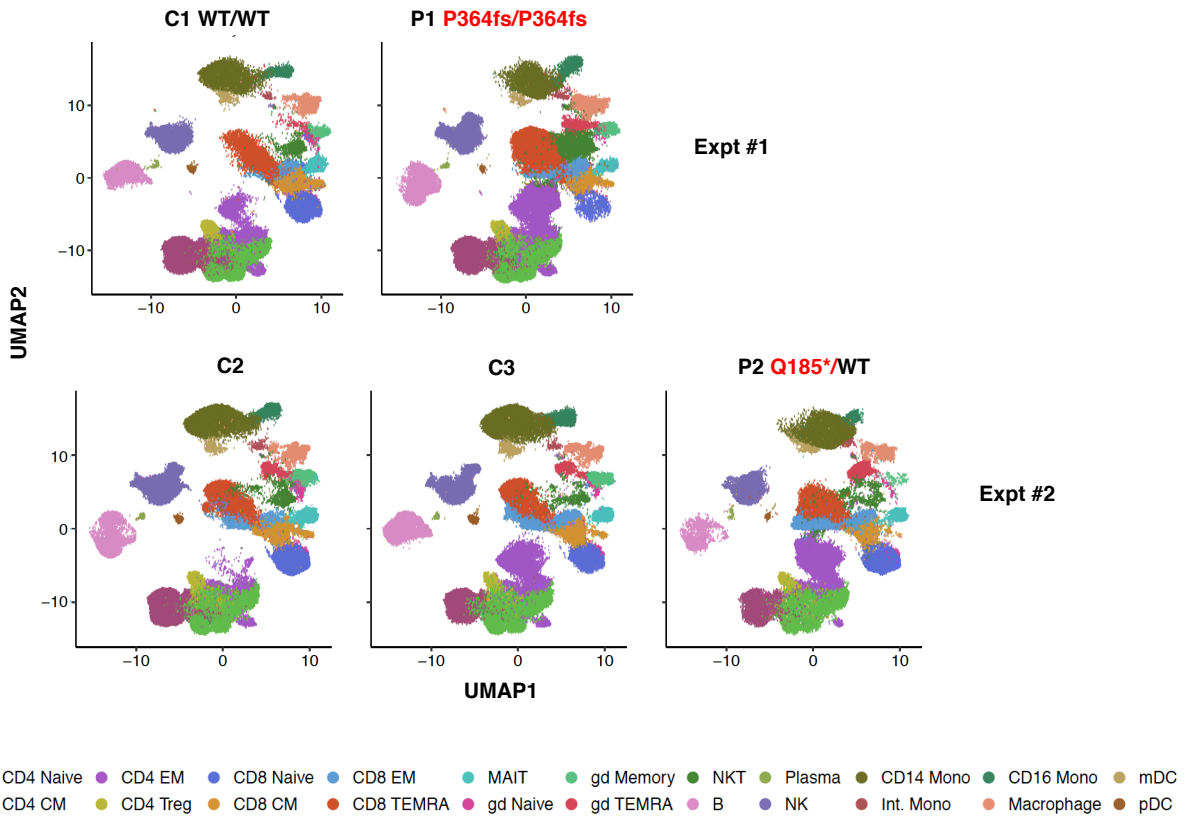
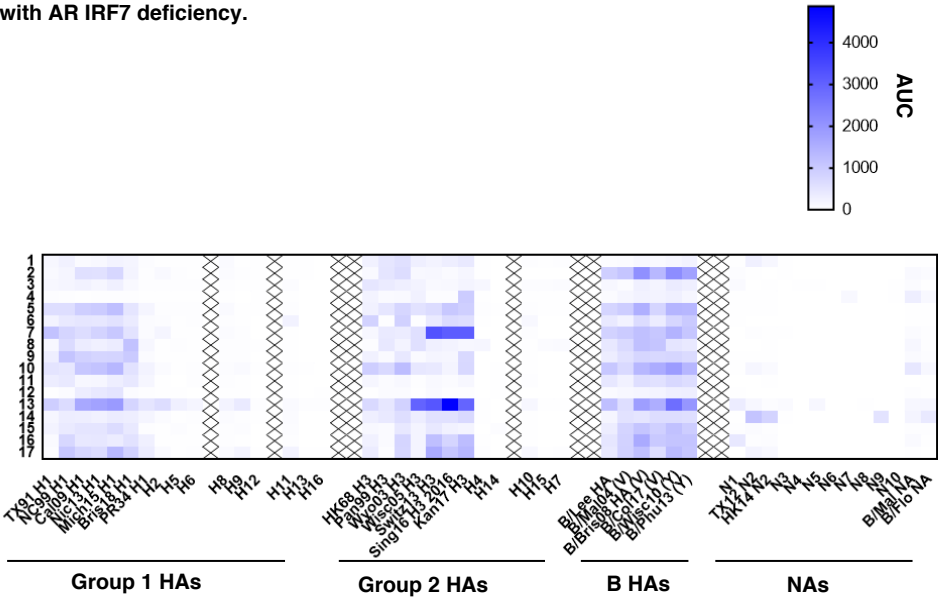


Fig. S10. IAV exposure in a patient with AR IRF7 deficiency.

A

- 1. Sister (IRF7 WT/WT)
- 2. C1
- 3. IRF7 P364fs/P364fs sample 1
- 4. C2
- 5. C3
- 6. IRF7 P364fs/P364fs sample 2
- 7. Father (IRF7 P364fs/WT)
- 8. C4
- 9. C5
- 10. C6
- 11. C7
- 12. C8
- 13. Mother (IRF7 P364fs/WT)
- 14. Brother (IRF7 P364fs/WT)
- 15. C9
- 16. C10
- 17. Travel control



B

Lable	Key
PR34 H1	A/Puerto Rico/8/34 (H1N1)
TX91 H1	A/Texas/36/91 (H1N1)
NC99 H1	A/New Caledonia/20/1999 (H1)
Cal09 H1	A/California/04/2009 (H1N1)
Mich15 H1	A/Michigan/45/2015 (H1)
Nic13 H1	A/Nicaragua/1815_01_TR2/2013 H1
Bris18 H1	A/Brisbane/02/2018 (H1)
H2	A/Japan/305/57 (H2N2)
H5	A/Indonesia/05/2005 (H5)
H6	A/mallard/Sweden/81/02 (H6N4)
H11	A/shoveler/Netherlands/18/99 (H11N9)
H16	A/black headed gull/Sweden/5/99 (H16N3)
H13	A/black headed gull/Sweden/1/1999 (H13)
H8	A/mallard/Sweden/24/2002 (H8)
H12	A/mallard/Interior Alaska/7MP0167/2007 (H12)
H9	A/guinea fowl/Hong Kong/WF10/1999 (H9)
HK68 H3	A/Hong Kong/1/1968 (H3)
Pan99 H3	A/Panama/2007/1999 (H3)
Wisc05 H3	A/Wisconsin/67/2005 (H3)
Wyo03 H3	A/Wyoming/3/2003 (H3)
Switz13 H3	A/Switzerland/9715293/2013 (H3N2)
Sing16 H3 2016	A/Singapore/INFIMH-16-0019/2016 (H3)
Kan17 H3	A/Kansas/14/2017 (H3)
H4	A/red knot/Delaware/541/1988 (H4)
H14	A/mallard/Gurjev/263/82 (H14N5)
H10	A/mallard/Interior Alaska/10BM01929/2010 (H10)
H7	A/chicken/BC/CN-6/04 (H7)
H15	A/shearwater/West Australia/2576/1979 (H15)
B/Wisc10 (Y)	B/Wisconsin/1/2010 (B-HA)
B/Bris08 HA (V)	B/Brisbane/60/2008 (B-HA)
B/Mal04 (V)	B/Malaysia/2506/2004 (B-HA)
B/Phu13 (Y)	B/Phuket/3073/2013 (B-HA)
B/Col17 (V)	B/Colorado/06/2017 (B-HA)
B/Lee HA	B/Lee/1940 (B-HA)

Fig. S11. Virscan analysis of a patient with an AR IRF7 deficiency.

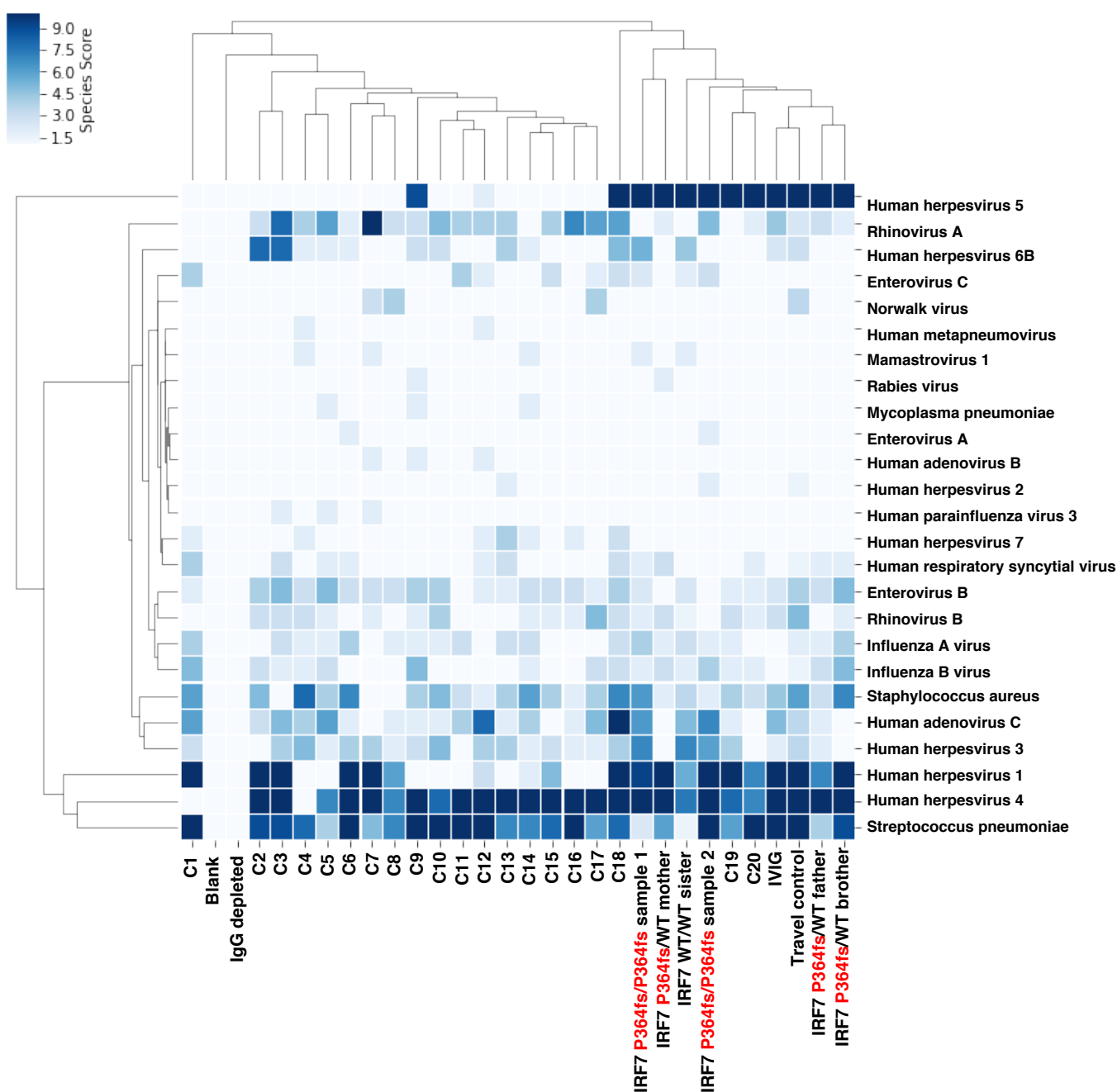


Table S1. Variants of the 12 autosomal loci identified in patients with life-threatening COVID-19.

Gene	Chromosome	Position (GRCh37)	Reference	Altered	Genotype	Zygosity	Predicted LOF	Function	Number of patients
TLR3	4	187003591	C	G	p.Arg251Gly	het		hypomorph	1
TLR3	4	187005020	A	G	p.Met870Val	het		LOF	1
TLR3	4	187005034	T	C	p.Phe732Leu	het		neutral	1
TLR3	4	187004500	C	T	p.Pro554Ser	het		LOF	1
TLR3	4	186998173	C	C	p.Ser134Pro	het		neutral	1
TLR3	4	187003852	AT	A	p.Ser339fs	het	pLOF	LOF	1
TLR3	4	187005146	G	A	p.Trp769*	het	pLOF	LOF	1
UNC93B1	11	67763289	C	T	p.Ala385Thr	het		neutral	1
UNC93B1	11	67763138	T	C	p.Tyr435Cys	het		neutral	1
UNC93B1	11	67763307	C	T	p.Val379Met	het		neutral	1
UNC93B1	11	67764078	C	T	p.Ala361Thr	het		neutral	1
UNC93B1	11	67770598	C	A	p.Glu96*	het	pLOF	LOE	1
UNC93B1	11	67759034	C	T	p.Gly592Arg	het		neutral	2
UNC93B1	11	67767052	G	A	p.Ser164Leu	het		neutral	1
UNC93B1	11	67763238	C	G	p.Val402Leu	het		neutral	1
UNC93B1	11	67759150	C	T	p.Gly553Asp	het		neutral	1
TICAM1	19	4817486	C	G	p.Val302Leu	het		neutral	1
TICAM1	19	4818059	C	T	p.Ala111Thr	het		neutral	1
TICAM1	19	4818178	C	T	p.Arg71Gln	het		neutral	3
TICAM1	19	4816721	C	T	p.Asp557Asn	het		neutral	1
TICAM1	19	4817216	C	A	p.Gln392Lys	het		LOF	1
TICAM1	19	4816285	T	C	p.Gln702Arg	het		neutral	1
TICAM1	19	4816598	C	A	p.Gly598Trp	het		neutral	1
TICAM1	19	4817233	A	G	p.Leu386Pro	het		neutral	1
TICAM1	19	4816607	T	A	p.Met595Leu	het		neutral	1
TICAM1	19	4816996	C	T	p.Ser465Asn	het		neutral	1
TICAM1	19	4818211	G	C	p.Ser60Cys	het		LOF	1
TICAM1	19	4817920	G	A	p.Thr157Met	het		neutral	1
TICAM1	19	4817260	G	A	p.Thr377Ile	het		neutral	1
TICAM1	19	4818379	G	A	p.Thr41le	het		LOF	1
TICAM1	19	4818152	C	T	p.Val80Met	het		neutral	1
TRAF3	14	103342855	C	T	p.Ala188Val	het		neutral	1
TRAF3	14	103371648	G	A	p.Ala412Thr	het		neutral	1
TRAF3	14	103369593	G	A	p.Arg321Gln	het		neutral	1
TRAF3	14	103357733	G	A	p.Trp366Cys	het		neutral	1
TRAF3	14	103355963	G	A	p.Val240Ile	het		neutral	1
TRAF3	14	103369730	G	A	p.Val367Met	het		neutral	1
TBK1	12	64878253	A	G	p.Asn388Ser	het		neutral	1
TBK1	12	64889344	G	A	p.Ala535Thr	het		neutral	1
TBK1	12	64875731	T	T	p.Arg308*	het	pLOF	LOF	1
TBK1	12	64891037	G	C	p.Glu653Gln	het		neutral	1
TBK1	12	64879235	T	C	p.Ile397Thr	het		neutral	2
TBK1	12	64889307	G	C	p.Ile522Met	het		neutral	1
TBK1	12	64889263	C	A	p.Leu508Ile	het		neutral	1
TBK1	12	64849721	T	C	p.Phe245Ser	het		LOF	1
TBK1	12	64891443	C	T	p.Pro659Ser	het		neutral	1
TBK1	12	64860776	G	C	p.Val152Leu	het		neutral	1
TBK1	12	64878241	G	A	p.Arg384Gln	het		neutral	1
IRF3	19	50165507	C	T	p.Arg227Gln	het		neutral	1
IRF3	19	50164059	C	T	p.Gly337Arg	het		hypomorph	1
IRF3	19	50165845	C	C	p.Asn146Lys	het		HYPO	1
IRF3	19	50167946	ATCC	A	p.Glu49del	het		HYPO	1
IRF3	19	50162988	G	C	p.Leu401Val	het		neutral	1
IRF7	11	615095	A	C	p.Arg7fs	het	pLOF	LOF	1
IRF7	11	613100	C	T	p.Ala419Thr	het		neutral	1
IRF7	11	614799	C	T	p.Arg131Gln	het		neutral #	4
IRF7	11	613337	C	T	p.Arg369Gln	het		HYPO	1
IRF7	11	613087	G	G	p.Arg423Pro	het		neutral	1
IRF7	11	615170	T	T	p.Arg37His	het		neutral	1
IRF7	11	614842	C	T	p.Asp117Asn	het		HYPO	1
IRF7	11	614300	G	A	p.Gln185*	het	pLOF	LOF	1
IRF7	11	614532	C	G	p.Gly133Arg	het		neutral	1
IRF7	11	614212	C	T	p.Gly214Glu	het		neutral	1
IRF7	11	613978	C	T	p.Gly247Arg	het		neutral #	4
IRF7	11	613332	T	C	p.Met371Val	het		LOF	1
IRF7	11	614907	A	G	p.Phe95Ser	het		LOF	1
IRF7	11	613966	CGGGCTGGGGCCCCG	C	p.Pro246fs	het	pLOF	HYPO	1
IRF7	11	613353	G	GC	p.Pro364fs	hom	pLOF	HYPO	1
IRF7	11	613957	T	C	p.Thr254Ala	het		neutral	1
IFNAR1	21	34697431	C	T	p.Ala24Val	het		neutral	2
IFNAR1	21	34725190	G	A	p.Ala424Thr	het		neutral	1
IFNAR1	21	34713367	A	G	p.Asn88Ser	het		neutral	1
IFNAR1	21	34713344	G	C	p.Gln80His	het		neutral	1
IFNAR1	21	34725076	G	C	p.Glu386Lys	het		neutral	1
IFNAR1	21	34727724	G	A	p.Glu515Lys	het		neutral	1
IFNAR1	21	34715704	C	G	p.Ile169Met	het		neutral	1
IFNAR1	21	34715856	A	G	p.Ile183Val	het		neutral	1
IFNAR1	21	34721704	TTCC	T	p.Pro335del	het		LOF	1
IFNAR1	21	34713351	A	G	p.Thr83Ala	het		neutral	1
IFNAR1	21	34713323	G	C	p.Trp73Cys	hom		LOF	1
IFNAR1	21	34725184	A	C	p.Ser422Arg	hom		LOF	1
IFNAR1	21	34721524	C	T	p.Arg306Cys	het		N.T.	1
IFNAR1	21	34721527	G	A	p.Val307Ile	het		N.T.	1
IFNAR1	21	34707922	G	A	p.Gly57Arg	het		neutral	1
IFNAR2	21	34621033	G	GTCT	p.Glu138_Phe139insSer	het		N.T.	1
IFNAR2	21	34621032	A	T	p.Glu138Val	het		neutral	1
IFNAR2	21	34621038	AGATTGTTGGTTTT	A	p.Glu140fs	het	pLOF	LOF	1
IFNAR2	21	34617267	G	C	p.Glu37Gln	het		neutral	2
IFNAR2	21	34635105	A	G	p.His283Arg	het		neutral	1
IFNAR2	21	34625016	T	C	p.Ile197Thr	het		neutral	1
IFNAR2	21	34617375	A	G	p.Met75Val	het		neutral	1
IFNAR2	21	34635141	C	T	p.Pro295Leu	het		neutral	1
IFNAR2	21	34635293	C	T	p.Pro346Ser	het		neutral	1
IFNAR2	21	34635341	C	T	p.Pro362Ser	het		neutral	1
IFNAR2	21	34635411	C	T	p.Pro385Leu	het		neutral	1
IFNAR2	21	34625069	A	G	p.Ser215Gly	het		neutral	1
IFNAR2	21	34635228	G	A	p.Ser324Asn	het		neutral	2
IFNAR2	21	34635606	C	T	p.Ser450Leu	het		neutral	1
IFNAR2	21	34635210	A	G	p.Trp318Cys	het		neutral	1
STAT1	2	191843670	C	A	p.Ser485Thr	het		neutral	1
STAT1	2	191845387	C	T	p.Ala531Thr	het		N.T.	1
STAT1	2	191859938	T	C	p.Ile265Val	het		N.T.	1
STAT1	2	191847238	A	T	p.Gln595His	het		neutral	1
STAT2	12	56749227	C	G	p.Glu157Asp	het		neutral	1
STAT2	12	56749951	G	A	p.Gln84Lys	het		neutral	1
STAT2	12	56742818	G	T	p.Pro489Leu	het		neutral	1
STAT2	12	56737358	G	C	p.Ala824Gly	het		neutral	1
STAT2	12	56740704	C	T	p.Arg587His	het		neutral	1
STAT2	12	56743042	C	T	p.Asp449Asn	het		neutral	1
STAT2	12	56748338	G	T	p.Leu232Met	het		neutral	1
STAT2	12	56737650	A	C	p.Leu791Trp	het		neutral	1
STAT2	12	56742818	G	T	p.Pro489His	het		neutral	1
STAT2	12	56737831	G	A	p.Pro731Ser	het		neutral	1
STAT2	12	56750247	G	A	p.Val439Phe	het		neutral	1
IRF9	14	24633220	A	G	p.Glu209Gly	het		neutral	1
IRF9	14	24633301	C	A	p.Gly203Arg	het		neutral	1
IRF9	14	24632680	C	T	p.Thr153Ile	het		neutral	1
IRF9	14	24633861	G	A	p.Val230Met	het		neutral	1

§ c.438C>G leads to both p.Asn146Lys (hypomorph) and a cryptic splicing site (p.G145_E20del, hypomorph) (Fig S3).

known neutral variants (reference #7)

het: heterozygous

hom: homozygous

LOF: loss-of-function

LOE: loss-of-expression

HYPO: severely hypomorph

N.T.: Not tested

Table S2. Variants identified in the 417 known ILL-causing genes in patients with defects of the type 1778 pathway.

Disorder	Number	Position	Variant ID	Reference Nucleotide	Altered Nucleotide	Function	Gene	Transcript ID	Amino Acid Change	Zygosity	Frequency	Frequency	Combined Annotation Dismant	Depletion (CADD) V1.3	Mutation Significance Cutoff (NSC)	Mutation Significance Cutoff (NSC)	Mutation Significance Cutoff (NSC)	Gene Damage Index (GDI)	Variant Quality	Known genetic form
AD P/NM1 (p.Pro155del)	4	126239377	n170704466	T	G	missense	FA14	ENCT00000094120	p.Val161Glu	het	0	3.22E-05	21.08	0	HIGH	24.85	780	AR		
AD P/NM1 (p.Pro155del)	4	126239359	-	T	A	missense	FA14	ENCT00000094129	p.Val118Ala	het	0	26.4	0	HIGH	24.85	652	AR			
AD P/NM1 (p.Pro155del)	26	82388528	n1754014807	G	A	missense	PC12	ENCT00000099376	p.Val120Glu	het	3.88E-05	8.02E-05	17.84	2.31	HIGH	5.25	667	AD GCF		
AD TLR3 (p.Pro554Ser)	2	1615144765	-	C	T	missense	IFIH1	ENCT000000043642	p.Ala110Thr	het	0	24	0	10.33	HIGH	11.41	818	AD GCF or AR		
AD RFX1 (p.Asn146Asp)	6	90942255	n1021039587	G	A	missense	EAC2D	ENCT000000021749	p.Pro180Leu	het	2.23E-04	2.07E-04	11.31	2.31	HIGH	2.54	327	AD GCF		
AD RFX1 (p.Arg395Gln)	12	494321729	n170788910	A	A>G>	indel (frameshift)	KMT2D	ENCT00000002087	p.Gln187Stop	het	4.42E-04	1.98E-04	0	0	HIGH	6.74	776	AD		
AR P/NM1 (p.Ser422Arg)	12	49431110	-	G	T	missense	KMT2D	ENCT00000002087	p.Pro1317Asn	het	0	0	22.8	0	HIGH	6.74	24	AD		
AR P/NM1 (p.Ser422Arg)	12	49431103	-	A	G	missense	KMT2D	ENCT00000002087	p.Pro2408Ser	het	0	0	22.9	0	HIGH	6.74	20	AD		
AR P/NM1 (p.Ser422Arg)	2	203831386	-	A	C	missense	KANBF2	ENCT000000028195	p.Thr151Ile	het	0	0	0.05	0.05	HIGH	6.15	36	AD		
AR RFX1 (p.Pro146Leu)	2	109171205	-	A	C	missense	KANBF2	ENCT000000028195	p.Thr178Pro	het	0	0	22.1	0.03	HIGH	6.15	1992	AD		
AD RFX1 (p.Gln185*)	6	31817883	n1229029793	G	A	missense	CFB	ENCT000000042168	p.Arg188Asn	het	0	1.62E-05	20.8	0	HIGH	4.88	2547	AD or AR		
AD RFX1 (p.Gln185*)	3	103584413	n136460539	G	A	missense	FAHAF3	ENCT000000031325	p.Arg147Pro	het	0	0.05E-06	21.8	0.03	HIGH	6.15	5171	AD		
AR P/NM1 (p.Tyr170Val)	7	92781991	n1747865043	C	G	missense	SAMD9L	ENCT000000182188	p.Ala142Pro	het	0	7.88E-06	24.8	2.31	HIGH	5.15	439	AD (GCF)		
AR RFX1 (p.Met171Val/p.Arg121Ile)	13	6401293	n126891378	C	T	missense	TRIPAP1A	ENCT000000162749	p.Val121Met	het	0.00E+00	2.37E-04	30	0.03	HIGH	3.13	731	AD		
AD RFX1 (p.Pro146Asp)	15	77323479	n126125312	C	T	missense	PSTRP1	ENCT000000158612	p.Arg455Gln	het	5.79E-04	5.68E-04	21.8	13.54	HIGH	3.21	542	AD		
AD UNC3B1 (p.Glu169*)	2	15427125	n148464908	G	A	missense	NBA5	ENCT000000028113	p.Val171Met	het	6.87E-05	2.85E-04	26.1	2.31	HIGH	2.23	805	AR		
AD UNC3B1 (p.Glu169*)	2	154274637	-	A	C	missense	NBA5	ENCT000000028113	p.Tyr155Glu	het	0	0	26.1	2.31	HIGH	9.7	810	AR		
AD UNC3B1 (p.Glu169*)	8	2621896	-	A	G	missense	PABPF2	ENCT000000101383	p.Tyr120Val	het	0	0	24.8	0	HIGH	2.23	806	AD		
AD UNC3B1 (p.Glu169*)	8	208118129	-	A	C	missense	PABPF2	ENCT000000101383	p.Asn121Ile	het	0	0	14.86	0	HIGH	21.5	456	AD		
AD UNC3B1 (p.Glu169*)	8	100711889	-	C	CA	indel (frameshift)	VPS13B	ENCT000000105844	p.Asn108Pro	het	0	0	22.6	0	HIGH	15.5	386	AR		
AD TLR1 (p.Pro24Ser)	7	92781441	n1772610240	G	A	missense	SAMD6L	ENCT000000182188	p.Val187Pro	het	0	3.99E-06	26.1	2.31	HIGH	5.15	680	AD (GCF)		
AD TLR1 (p.Pro24Ser)	9	396687	n14284120	G	A	missense	DOK8	ENCT000000041881	p.Arg120Gln	het	7.33E-04	7.12E-04	35	0	HIGH	18.29	972	AR		
AD TLR1 (p.Pro24Ser)	9	401895	n138910988	G	C	missense	DOK8	ENCT000000041881	p.Gln120Arg	het	7.02E-04	7.04E-04	21.4	0	HIGH	18.29	529	AR		
AD TLR1 (p.Ser159Leu)	29	6707125	n139919128	G	T	missense	CFI	ENCT000000049367	p.Ala67Thr	het	0	1.21E-05	0	0.18	HIGH	4.44	410	AD or AR		
AD TLR1 (p.Arg387)	16	3251467	n61752177	T	C	missense	MIRF1	ENCT000000109586	p.Ser69Gln	het	1.82E-04	2.82E-04	10.01	0	HIGH	7.13	6810	AD or AR		
AD TLR3 (p.Tyr767*)	1	234744729	n150476155	A	G	missense	IRF3B2	ENCT000000166609	p.Val173Pro	het	0	1.08E-05	13.28	2.31	HIGH	4.9	4910	AD		
AD TLR3 (p.Tyr767*)	6	13822185	n136802129	G	A	missense	TNFAIP3	ENCT000000171789	p.Arg763Pro	het	1.20E-05	7.41E-05	25.3	2.31	HIGH	6.54	6516	AD (GCF)		
AD TLR3 (p.Tyr767*)	8	61714300	n179218763	C	A	missense	CHOP	ENCT0000000418902	p.Glu154Asp	het	0	8.10E-06	33	0.07	HIGH	4.77	646	AD		

AD: autosomal dominant

AR: autosomal recessive

GCF: gain-of-function

References and Notes

1. D. M. Morens, A. S. Fauci, Emerging pandemic diseases: How we got to COVID-19. *Cell* **182**, 1077–1092 (2020). [doi:10.1016/j.cell.2020.08.021](https://doi.org/10.1016/j.cell.2020.08.021) [Medline](#)
2. J. L. Casanova, L. Abel, Lethal Infectious Diseases as Inborn Errors of Immunity: Toward a Synthesis of the Germ and Genetic Theories. *Annu. Rev. Pathol.* (2020). [Medline](#)
3. J. L. Casanova, L. Abel, The human genetic determinism of life-threatening infectious diseases: Genetic heterogeneity and physiological homogeneity? *Hum. Genet.* **139**, 681–694 (2020). [doi:10.1007/s00439-020-02184-w](https://doi.org/10.1007/s00439-020-02184-w) [Medline](#)
4. J. L. Casanova, H. C. Su; COVID Human Genetic Effort, A global effort to define the human genetics of protective immunity to SARS-CoV-2 infection. *Cell* **181**, 1194–1199 (2020). [doi:10.1016/j.cell.2020.05.016](https://doi.org/10.1016/j.cell.2020.05.016) [Medline](#)
5. Q. Zhang, Human genetics of life-threatening influenza pneumonitis. *Hum. Genet.* **139**, 941–948 (2020). [doi:10.1007/s00439-019-02108-3](https://doi.org/10.1007/s00439-019-02108-3) [Medline](#)
6. H. K. Lim, S. X. L. Huang, J. Chen, G. Kerner, O. Gilliaux, P. Bastard, K. Dobbs, N. Hernandez, N. Goudin, M. L. Hasek, E. J. García Reino, F. G. Lafaille, L. Lorenzo, P. Luthra, T. Kochetkov, B. Bigio, S. Boucherit, F. Rozenberg, C. Vedrinne, M. D. Keller, Y. Itan, A. García-Sastre, M. Celard, J. S. Orange, M. J. Ciancanelli, I. Meyts, Q. Zhang, L. Abel, L. D. Notarangelo, H.-W. Snoeck, J.-L. Casanova, S.-Y. Zhang, Severe influenza pneumonitis in children with inherited TLR3 deficiency. *J. Exp. Med.* **216**, 2038–2056 (2019). [doi:10.1084/jem.20181621](https://doi.org/10.1084/jem.20181621) [Medline](#)
7. M. J. Ciancanelli, S. X. L. Huang, P. Luthra, H. Garner, Y. Itan, S. Volpi, F. G. Lafaille, C. Trouillet, M. Schmolke, R. A. Albrecht, E. Israelsson, H. K. Lim, M. Casadio, T. Hermesh, L. Lorenzo, L. W. Leung, V. Pedernana, B. Boisson, S. Okada, C. Picard, B. Ringuier, F. Troussier, D. Chaussabel, L. Abel, I. Pellier, L. D. Notarangelo, A. García-Sastre, C. F. Basler, F. Geissmann, S.-Y. Zhang, H.-W. Snoeck, J.-L. Casanova, Life-threatening influenza and impaired interferon amplification in human IRF7 deficiency. *Science* **348**, 448–453 (2015). [doi:10.1126/science.aaa1578](https://doi.org/10.1126/science.aaa1578) [Medline](#)
8. N. Hernandez, I. Melki, H. Jing, T. Habib, S. S. Y. Huang, J. Danielson, T. Kula, S. Drutman, S. Belkaya, V. Rattina, L. Lorenzo-Diaz, A. Boulai, Y. Rose, N. Kitabayashi, M. P. Rodero, C. Dumaine, S. Blanche, M.-N. Lebras, M. C. Leung, L. S. Mathew, B. Boisson, S.-Y. Zhang, S. Boisson-Dupuis, S. Giliani, D. Chaussabel, L. D. Notarangelo, S. J. Elledge, M. J. Ciancanelli, L. Abel, Q. Zhang, N. Marr, Y. J. Crow, H. C. Su, J.-L. Casanova, Life-threatening influenza pneumonitis in a child with inherited IRF9 deficiency. *J. Exp. Med.* **215**, 2567–2585 (2018). [doi:10.1084/jem.20180628](https://doi.org/10.1084/jem.20180628) [Medline](#)
9. V. Sancho-Shimizu, R. Pérez de Diego, L. Lorenzo, R. Halwani, A. Alangari, E. Israelsson, S. Fabrega, A. Cardon, J. Maluenda, M. Tatematsu, F. Mahvelati, M. Herman, M. Ciancanelli, Y. Guo, Z. AlSum, N. Alkhamis, A. S. Al-Makadma, A. Ghadiri, S. Boucherit, S. Plancoulaine, C. Picard, F. Rozenberg, M. Tardieu, P. Lebon, E. Jouanguy, N. Rezaei, T. Seya, M. Matsumoto, D. Chaussabel, A. Puel, S.-Y. Zhang, L. Abel, S. Al-Muhsen, J.-L. Casanova, Herpes simplex encephalitis in children with autosomal recessive and dominant TRIF deficiency. *J. Clin. Invest.* **121**, 4889–4902 (2011). [doi:10.1172/JCI59259](https://doi.org/10.1172/JCI59259) [Medline](#)

10. A. Casrouge, S.-Y. Zhang, C. Eidenschenk, E. Jouanguy, A. Puel, K. Yang, A. Alcais, C. Picard, N. Mahfoufi, N. Nicolas, L. Lorenzo, S. Plancoulaine, B. Sénéchal, F. Geissmann, K. Tabeta, K. Hoebe, X. Du, R. L. Miller, B. Héron, C. Mignot, T. B. de Villemeur, P. Lebon, O. Dulac, F. Rozenberg, B. Beutler, M. Tardieu, L. Abel, J.-L. Casanova, Herpes simplex virus encephalitis in human UNC-93B deficiency. *Science* **314**, 308–312 (2006). [doi:10.1126/science.1128346](https://doi.org/10.1126/science.1128346) [Medline](#)
11. R. Pérez de Diego, V. Sancho-Shimizu, L. Lorenzo, A. Puel, S. Plancoulaine, C. Picard, M. Herman, A. Cardon, A. Durandy, J. Bustamante, S. Vallabhapurapu, J. Bravo, K. Warnatz, Y. Chaix, F. Cascarrigny, P. Lebon, F. Rozenberg, M. Karin, M. Tardieu, S. Al-Muhsen, E. Jouanguy, S.-Y. Zhang, L. Abel, J.-L. Casanova, Human TRAF3 adaptor molecule deficiency leads to impaired Toll-like receptor 3 response and susceptibility to herpes simplex encephalitis. *Immunity* **33**, 400–411 (2010). [doi:10.1016/j.immuni.2010.08.014](https://doi.org/10.1016/j.immuni.2010.08.014) [Medline](#)
12. M. Herman, M. Ciancanelli, Y.-H. Ou, L. Lorenzo, M. Klaudel-Dreszler, E. Pauwels, V. Sancho-Shimizu, R. Pérez de Diego, A. Abhyankar, E. Israelsson, Y. Guo, A. Cardon, F. Rozenberg, P. Lebon, M. Tardieu, E. Heropolitańska-Pliszka, D. Chaussabel, M. A. White, L. Abel, S.-Y. Zhang, J.-L. Casanova, Heterozygous TBK1 mutations impair TLR3 immunity and underlie herpes simplex encephalitis of childhood. *J. Exp. Med.* **209**, 1567–1582 (2012). [doi:10.1084/jem.20111316](https://doi.org/10.1084/jem.20111316) [Medline](#)
13. L. L. Andersen, N. Mørk, L. S. Reinert, E. Kofod-Olsen, R. Narita, S. E. Jørgensen, K. A. Skipper, K. Höning, H. H. Gad, L. Østergaard, T. F. Ørntoft, V. Hornung, S. R. Paludan, J. G. Mikkelsen, T. Fujita, M. Christiansen, R. Hartmann, T. H. Mogensen, Functional IRF3 deficiency in a patient with herpes simplex encephalitis. *J. Exp. Med.* **212**, 1371–1379 (2015). [doi:10.1084/jem.20142274](https://doi.org/10.1084/jem.20142274) [Medline](#)
14. M. Audry, M. Ciancanelli, K. Yang, A. Cobat, H.-H. Chang, V. Sancho-Shimizu, L. Lorenzo, T. Niehues, J. Reichenbach, X.-X. Li, A. Israel, L. Abel, J.-L. Casanova, S.-Y. Zhang, E. Jouanguy, A. Puel, NEMO is a key component of NF- κ B- and IRF-3-dependent TLR3-mediated immunity to herpes simplex virus. *J. Allergy Clin. Immunol.* **128**, 610–617.e4 (2011). [doi:10.1016/j.jaci.2011.04.059](https://doi.org/10.1016/j.jaci.2011.04.059) [Medline](#)
15. N. Hernandez, G. Bucciol, L. Moens, J. Le Pen, M. Shahrooei, E. Goudouris, A. Shirkani, M. Changi-Ashtiani, H. Rokni-Zadeh, E. H. Sayar, I. Reisli, A. Lefevre-Utile, D. Zijlmans, A. Jurado, R. Pholien, S. Drutman, S. Belkaya, A. Cobat, R. Boudewijns, D. Jochmans, J. Neyts, Y. Seeleuthner, L. Lorenzo-Diaz, C. Enemchukwu, I. Tietjen, H.-H. Hoffmann, M. Momenilandi, L. Pöyhönen, M. M. Siqueira, S. M. B. de Lima, D. C. de Souza Matos, A. Homma, M. L. S. Maia, T. A. da Costa Barros, P. M. N. de Oliveira, E. C. Mesquita, R. Gijssbers, S.-Y. Zhang, S. J. Seligman, L. Abel, P. Hertzog, N. Marr, R. M. Martins, I. Meyts, Q. Zhang, M. R. MacDonald, C. M. Rice, J.-L. Casanova, E. Jouanguy, X. Bossuyt, Inherited IFNAR1 deficiency in otherwise healthy patients with adverse reaction to measles and yellow fever live vaccines. *J. Exp. Med.* **216**, 2057–2070 (2019). [doi:10.1084/jem.20182295](https://doi.org/10.1084/jem.20182295) [Medline](#)
16. C. J. Duncan, S. M. B. Mohamad, D. F. Young, A. J. Skelton, T. R. Leahy, D. C. Munday, K. M. Butler, S. Morfopoulou, J. R. Brown, M. Hubank, J. Connell, P. J. Gavin, C. McMahon, E. Dempsey, N. E. Lynch, T. S. Jacques, M. Valappil, A. J. Cant, J. Breuer, K. R. Engelhardt, R. E. Randall, S. Hambleton, Human IFNAR2 deficiency: Lessons for

- antiviral immunity. *Sci. Transl. Med.* **7**, 307ra154 (2015).
[doi:10.1126/scitranslmed.aac4227](https://doi.org/10.1126/scitranslmed.aac4227) [Medline](#)
17. S. Dupuis, E. Jouanguy, S. Al-Hajjar, C. Fieschi, I. Z. Al-Mohsen, S. Al-Jumaah, K. Yang, A. Chapgier, C. Eidenschenk, P. Eid, A. Al Ghonaium, H. Tufenkeji, H. Frayha, S. Al-Gazlan, H. Al-Rayes, R. D. Schreiber, I. Gresser, J.-L. Casanova, Impaired response to interferon-alpha/beta and lethal viral disease in human STAT1 deficiency. *Nat. Genet.* **33**, 388–391 (2003). [doi:10.1038/ng1097](https://doi.org/10.1038/ng1097) [Medline](#)
 18. S. Hambleton, S. Goodbourn, D. F. Young, P. Dickinson, S. M. B. Mohamad, M. Valappil, N. McGovern, A. J. Cant, S. J. Hackett, P. Ghazal, N. V. Morgan, R. E. Randall, STAT2 deficiency and susceptibility to viral illness in humans. *Proc. Natl. Acad. Sci. U.S.A.* **110**, 3053–3058 (2013). [doi:10.1073/pnas.1220098110](https://doi.org/10.1073/pnas.1220098110) [Medline](#)
 19. R. Döffinger, A. Smahi, C. Bessia, F. Geissmann, J. Feinberg, A. Durandy, C. Bodemer, S. Kenwrick, S. Dupuis-Girod, S. Blanche, P. Wood, S. H. Rabia, D. J. Headon, P. A. Overbeek, F. Le Deist, S. M. Holland, K. Belani, D. S. Kumararatne, A. Fischer, R. Shapiro, M. E. Conley, E. Reimund, H. Kalhoff, M. Abinun, A. Munnich, A. Israël, G. Courtois, J.-L. Casanova, X-linked anhidrotic ectodermal dysplasia with immunodeficiency is caused by impaired NF-kappaB signaling. *Nat. Genet.* **27**, 277–285 (2001). [doi:10.1038/85837](https://doi.org/10.1038/85837) [Medline](#)
 20. S. Y. Zhang, E. Jouanguy, S. Ugolini, A. Smahi, G. Elain, P. Romero, D. Segal, V. Sancho-Shimizu, L. Lorenzo, A. Puel, C. Picard, A. Chapgier, S. Plancoulaine, M. Titeux, C. Cognet, H. von Bernuth, C.-L. Ku, A. Casrouge, X.-X. Zhang, L. Barreiro, J. Leonard, C. Hamilton, P. Lebon, B. Héron, L. Vallée, L. Quintana-Murci, A. Hovnanian, F. Rozenberg, E. Vivier, F. Geissmann, M. Tardieu, L. Abel, J.-L. Casanova, TLR3 deficiency in patients with herpes simplex encephalitis. *Science* **317**, 1522–1527 (2007).
[doi:10.1126/science.1139522](https://doi.org/10.1126/science.1139522) [Medline](#)
 21. G. Zhang, N. A. deWeerd, S. A. Stifter, L. Liu, B. Zhou, W. Wang, Y. Zhou, B. Ying, X. Hu, A. Y. Matthews, M. Ellis, J. A. Triccas, P. J. Hertzog, W. J. Britton, X. Chen, C. G. Feng, A proline deletion in IFNAR1 impairs IFN-signaling and underlies increased resistance to tuberculosis in humans. *Nat. Commun.* **9**, 85 (2018). [doi:10.1038/s41467-017-02611-z](https://doi.org/10.1038/s41467-017-02611-z) [Medline](#)
 22. M. M. Thomsen, S. E. Jørgensen, M. Storgaard, L. S. Kristensen, J. Gjedsted, M. Christiansen, H. H. Gad, R. Hartmann, T. H. Mogensen, Identification of an IRF3 variant and defective antiviral interferon responses in a patient with severe influenza. *Eur. J. Immunol.* **49**, 2111–2114 (2019). [doi:10.1002/eji.201848083](https://doi.org/10.1002/eji.201848083) [Medline](#)
 23. M. M. Thomsen, S. E. Jørgensen, H. H. Gad, M. Storgaard, J. Gjedsted, M. Christiansen, R. Hartmann, T. H. Mogensen, Defective interferon priming and impaired antiviral responses in a patient with an IRF7 variant and severe influenza. *Med. Microbiol. Immunol. (Berl.)* **208**, 869–876 (2019). [doi:10.1007/s00430-019-00623-8](https://doi.org/10.1007/s00430-019-00623-8) [Medline](#)
 24. S. G. Tangye, W. Al-Herz, A. Bousfiha, T. Chatila, C. Cunningham-Rundles, A. Etzioni, J. L. Franco, S. M. Holland, C. Klein, T. Morio, H. D. Ochs, E. Oksenhendler, C. Picard, J. Puck, T. R. Torgerson, J.-L. Casanova, K. E. Sullivan, Human inborn errors of immunity: 2019 update on the classification from the International Union of Immunological

- Societies Expert Committee. *J. Clin. Immunol.* **40**, 24–64 (2020). [doi:10.1007/s10875-019-00737-x](https://doi.org/10.1007/s10875-019-00737-x) [Medline](#)
25. A. Bousfiha, L. Jeddane, C. Picard, W. Al-Herz, F. Ailal, T. Chatila, C. Cunningham-Rundles, A. Etzioni, J. L. Franco, S. M. Holland, C. Klein, T. Morio, H. D. Ochs, E. Oksenhendler, J. Puck, T. R. Torgerson, J.-L. Casanova, K. E. Sullivan, S. G. Tangye, Human Inborn Errors of Immunity: 2019 Update of the IUIS Phenotypical Classification. *J. Clin. Immunol.* **40**, 66–81 (2020). [doi:10.1007/s10875-020-00758-x](https://doi.org/10.1007/s10875-020-00758-x) [Medline](#)
 26. L. D. Notarangelo, R. Bacchetta, J.-L. Casanova, H. C. Su, Human inborn errors of immunity: An expanding universe. *Sci. Immunol.* **5**, eabb1662 (2020). [doi:10.1126/sciimmunol.abb1662](https://doi.org/10.1126/sciimmunol.abb1662) [Medline](#)
 27. J. Hadjadj, N. Yatim, L. Barnabei, A. Corneau, J. Boussier, N. Smith, H. Péré, B. Charbit, V. Bondet, C. Chenevier-Gobeaux, P. Breillat, N. Carlier, R. Gauzit, C. Morbieu, F. Pène, N. Marin, N. Roche, T.-A. Szwebel, S. H. Merkling, J.-M. Treluyer, D. Veyer, L. Mouthon, C. Blanc, P.-L. Tharaux, F. Rozenberg, A. Fischer, D. Duffy, F. Rieux-Laucat, S. Kernéis, B. Terrier, Impaired type I interferon activity and inflammatory responses in severe COVID-19 patients. *Science* **369**, 718–724 (2020). [doi:10.1126/science.abc6027](https://doi.org/10.1126/science.abc6027) [Medline](#)
 28. S. Trouillet-Assant, S. Viel, A. Gaymard, S. Pons, J.-C. Richard, M. Perret, M. Villard, K. Brengel-Pesce, B. Lina, M. Mezidi, L. Bitker, A. Belot; COVID HCL Study Group, Type I IFN immunoprofiling in COVID-19 patients. *J. Allergy Clin. Immunol.* **146**, 206–208.e2 (2020). [doi:10.1016/j.jaci.2020.04.029](https://doi.org/10.1016/j.jaci.2020.04.029) [Medline](#)
 29. P. Bastard, L. B. Rosen, Q. Zhang, E. Michailidis, H.-H. Hoffmann, Y. Zhang, K. Dorgham, Q. Philippot, J. Rosain, V. Béziat, J. Manry, E. Shaw, L. Haljasmägi, P. Peterson, L. Lorenzo, L. Bizien, S. Trouillet-Assant, K. Dobbs, A. Almeida de Jesus, A. Belot, A. Kallaste, E. Catherinot, Y. Tandjaoui-Lambiotte, J. Le Pen, G. Kerner, B. Bigio, Y. Seeleuthner, R. Yang, A. Bolze, A. N. Spaan, O. M. Delmonte, M. S. Abers, A. Aiuti, G. Casari, V. Lampasona, L. Piemonti, F. Ciceri, K. Bilguvar, R. P. Lifton, M. Vasse, D. M. Smadja, M. Migaud, J. Hadjadj, B. Terrier, D. Duffy, L. Quintana-Murci, D. van de Beek, L. Roussel, D. C. Vinh, S. G. Tangye, F. Haerynck, D. Dalmau, J. Martinez-Picado, P. Brodin, M. C. Nussenzweig, S. Boisson-Dupuis, C. Rodríguez-Gallego, G. Vogt, T. H. Mogensen, A. J. Oler, J. Gu, P. D. Burbelo, J. Cohen, A. Biondi, L. R. Bettini, M. D'Angio, P. Bonfanti, P. Rossignol, J. Mayaux, F. Rieux-Laucat, E. S. Husebye, F. Fusco, M. V. Ursini, L. Imberti, A. Sottini, S. Paghera, E. Quiros-Roldan, C. Rossi, R. Castagnoli, D. Montagna, A. Licari, G. L. Marseglia, X. Duval, J. Ghosn, HGID Lab, NIAID-USUHS Immune Response to COVID Group, COVID Clinicians, COVID-STORM Clinicians, Imagine COVID Group, French COVID Cohort Study Group, The Milieu Intérieur Consortium, CoV-Contact Cohort, Amsterdam UMC Covid-19 Biobank, COVID Human Genetic Effort, J. S. Tsang, R. Goldbach-Mansky, K. Kisand, M. S. Lionakis, A. Puel, S.-Y. Zhang, S. M. Holland, G. Gorochov, E. Jouanguy, C. M. Rice, A. Cobat, L. D. Notarangelo, L. Abel, H. C. Su, J.-L. Casanova, Auto-antibodies against type I IFNs in patients with life-threatening COVID-19. *Science* **10.1126/science.abd4585** (2020).
 30. M. A. DePristo, E. Banks, R. Poplin, K. V. Garimella, J. R. Maguire, C. Hartl, A. A. Philippakis, G. del Angel, M. A. Rivas, M. Hanna, A. McKenna, T. J. Fennell, A. M.

- Kernytsky, A. Y. Sivachenko, K. Cibulskis, S. B. Gabriel, D. Altshuler, M. J. Daly, A framework for variation discovery and genotyping using next-generation DNA sequencing data. *Nat. Genet.* **43**, 491–498 (2011). [doi:10.1038/ng.806](https://doi.org/10.1038/ng.806) [Medline](#)
31. H. Li, R. Durbin, Fast and accurate short read alignment with Burrows-Wheeler transform. *Bioinformatics* **25**, 1754–1760 (2009). [doi:10.1093/bioinformatics/btp324](https://doi.org/10.1093/bioinformatics/btp324) [Medline](#)
 32. B. Boisson, Y. Honda, M. Ajiro, J. Bustamante, M. Bendavid, A. R. Gennery, Y. Kawasaki, J. Ichishima, M. Osawa, H. Nihira, T. Shiba, T. Tanaka, M. Chrabieh, B. Bigio, H. Hur, Y. Itan, Y. Liang, S. Okada, K. Izawa, R. Nishikomori, O. Ohara, T. Heike, L. Abel, A. Puel, M. K. Saito, J.-L. Casanova, M. Hagiwara, T. Yasumi, Rescue of recurrent deep intronic mutation underlying cell type-dependent quantitative NEMO deficiency. *J. Clin. Invest.* **129**, 583–597 (2019). [doi:10.1172/JCI124011](https://doi.org/10.1172/JCI124011) [Medline](#)
 33. T. Gambin, Z. C. Akdemir, B. Yuan, S. Gu, T. Chiang, C. M. B. Carvalho, C. Shaw, S. Jhangiani, P. M. Boone, M. K. Eldomery, E. Karaca, Y. Bayram, A. Stray-Pedersen, D. Muzny, W. L. Charny, V. Bahrambeigi, J. W. Belmont, E. Boerwinkle, A. L. Beaudet, R. A. Gibbs, J. R. Lupski, Homozygous and hemizygous CNV detection from exome sequencing data in a Mendelian disease cohort. *Nucleic Acids Res.* **45**, 1633–1648 (2017). [Medline](#)
 34. D. Backenroth, J. Homsy, L. R. Murillo, J. Glessner, E. Lin, M. Brueckner, R. Lifton, E. Goldmuntz, W. K. Chung, Y. Shen, CANOES: Detecting rare copy number variants from whole exome sequencing data. *Nucleic Acids Res.* **42**, e97 (2014). [doi:10.1093/nar/gku345](https://doi.org/10.1093/nar/gku345) [Medline](#)
 35. M. Bouaziz, J. Mullaert, B. Bigio, Y. Seeleuthner, J.-L. Casanova, A. Alcais, L. Abel, A. Cobat, Controlling for human population stratification in rare variant association studies. *bioRxiv* 969477 [Preprint]. 28 February 2020. <https://doi.org/10.1101/2020.02.28.969477>.
 36. E. Persyn, R. Redon, L. Bellanger, C. Dina, The impact of a fine-scale population stratification on rare variant association test results. *PLOS ONE* **13**, e0207677 (2018). [doi:10.1371/journal.pone.0207677](https://doi.org/10.1371/journal.pone.0207677) [Medline](#)
 37. Y. Zhang, X. Shen, W. Pan, Adjusting for population stratification in a fine scale with principal components and sequencing data. *Genet. Epidemiol.* **37**, 787–801 (2013). [doi:10.1002/gepi.21764](https://doi.org/10.1002/gepi.21764) [Medline](#)
 38. S. Boisson-Dupuis, N. Ramirez-Alejo, Z. Li, E. Patin, G. Rao, G. Kerner, C. K. Lim, D. N. Kremensov, N. Hernandez, C. S. Ma, Q. Zhang, J. Markle, R. Martinez-Barricarte, K. Payne, R. Fisch, C. Deswarte, J. Halpern, M. Bouaziz, J. Mulwa, D. Sivanesan, T. Lazarov, R. Naves, P. Garcia, Y. Itan, B. Boisson, A. Checchi, F. Jabot-Hanin, A. Cobat, A. Guennoun, C. C. Jackson, S. Pekcan, Z. Caliskaner, J. Inostroza, B. T. Costa-Carvalho, J. A. T. de Albuquerque, H. Garcia-Ortiz, L. Orozco, T. Ozcelik, A. Abid, I. A. Rhorfi, H. Souhi, H. N. Amrani, A. Zegmout, F. Geissmann, S. W. Michnick, I. Muller-Fleckenstein, B. Fleckenstein, A. Puel, M. J. Ciancanelli, N. Marr, H. Abolhassani, M. E. Balcells, A. Condino-Neto, A. Strickler, K. Abarca, C. Teuscher, H. D. Ochs, I. Reisli, E. H. Sayar, J. El-Baghdadi, J. Bustamante, L. Hammarström, S. G. Tangye, S. Pellegrini, L. Quintana-Murci, L. Abel, J.-L. Casanova, Tuberculosis and impaired IL-23-dependent

- IFN- γ immunity in humans homozygous for a common *TYK2* missense variant. *Sci. Immunol.* **3**, eaau8714 (2018). [doi:10.1126/sciimmunol.aau8714](https://doi.org/10.1126/sciimmunol.aau8714) [Medline](#)
39. S. Fochi, E. Bergamo, M. Serena, S. Mutascio, C. Journo, R. Mahieux, V. Ciminale, U. Bertazzoni, D. Zipeto, M. G. Romanelli, TRAF3 Is Required for NF- κ B Pathway Activation Mediated by HTLV Tax Proteins. *Front. Microbiol.* **10**, 1302 (2019). [doi:10.3389/fmicb.2019.01302](https://doi.org/10.3389/fmicb.2019.01302) [Medline](#)
 40. D. F. Robbiani, C. Gaebler, F. Muecksch, J. C. C. Lorenzi, Z. Wang, A. Cho, M. Agudelo, C. O. Barnes, A. Gazumyan, S. Finkin, T. Hägglöf, T. Y. Oliveira, C. Viant, A. Hurley, H.-H. Hoffmann, K. G. Millard, R. G. Kost, M. Cipolla, K. Gordon, F. Bianchini, S. T. Chen, V. Ramos, R. Patel, J. Dizon, I. Shimeliovich, P. Mendoza, H. Hartweger, L. Nogueira, M. Pack, J. Horowitz, F. Schmidt, Y. Weisblum, E. Michailidis, A. W. Ashbrook, E. Waltari, J. E. Pak, K. E. Huey-Tubman, N. Koranda, P. R. Hoffman, A. P. West Jr., C. M. Rice, T. Hatziioannou, P. J. Bjorkman, P. D. Bieniasz, M. Caskey, M. C. Nussenzweig, Convergent antibody responses to SARS-CoV-2 in convalescent individuals. *Nature* **584**, 437–442 (2020). [doi:10.1038/s41586-020-2456-9](https://doi.org/10.1038/s41586-020-2456-9) [Medline](#)
 41. M. Ogishi, R. Yang, C. Gruber, S. Pelham, A. N. Spaan, J. Rosain, M. Chbihi, J. E. Han, V. K. Rao, L. Kainulainen, J. Bustamante, B. Boisson, D. Bogunovic, S. Boisson-Dupuis, J.-L. Casanova, Multi-batch cytometry data integration for optimal immunophenotyping. bioRxiv 202432 [Preprint]. 15 July 2020. <https://doi.org/10.1101/2020.07.14.202432>.
 42. P. Meade, G. Kuan, S. Strohmeier, H. E. Maier, F. Amanat, A. Balmaseda, K. Ito, E. Kirkpatrick, A. Javier, L. Gresh, R. Nachbagauer, A. Gordon, F. Krammer, Influenza virus infection induces a narrow antibody response in children but a broad recall response in adults. *mBio* **11**, e03243-19 (2020). [doi:10.1128/mBio.03243-19](https://doi.org/10.1128/mBio.03243-19) [Medline](#)